THE CASE FOR THE GLOBAL STRATOTYPE AND SECTION (GSSP) FOR THE BASE OF THE NORIAN STAGE

Mark W. Hounslow[1], and the Carnian-Norian boundary working group comprising: Gerhard H. Bachmann[2], Marco Balini[3], Mike J. Benton[4], Elizabeth E. Carter[5], Alexey G. Konstantinov[6], Martyn L. Golding[7], Leopold Krystyn[8], Wolfram Kuerschner[9], Spencer G. Lucas[10], Christopher A. McRoberts[11], Giovanni Muttoni[3], Alda Nicora[3], Tetsuji Onoue[12] Michael J. Orchard[7], Péter Ozsvárt[13], Niall W. Paterson[14], Sylvain Richoz[15], Manuel Rigo[16], Yadong Sun[17], Lydia S. Tackett[18], Ugar Kagan Tekin[19], Yongdong Wang[20], Yang Zhang[21], John-Paul Zonneveld[22].

1 LEC, Lancaster University, and Earth, Ocean and Ecological Sciences, University of Liverpool, UK
2. Institut für Geowissenschaften, Martin-Luther-Universität Halle-Wittenberg, D-06120 Halle (Saale), Germany
3 all'Università degli Studi di Milano,Il valore della ricerca interdisciplinare, Italy
4 University of Bristol, Life Sciences Building, Tyndall Avenue, Bristol, BS8 1TQ, UK
5 69745 Old Wagon Road, Sisters, OR 97759, USA
6 Trofimuk Inst. of Petro. Geology and Geophysics, Russian Academy of Sciences, Novosibirsk, 630090 Russia
7 Geological Survey of Canada, 1500-605 Robson Street, Vancouver, British Columbia V6B 5J3, Canada
8 Inst. Paleontology, Geozentrum UZA2, 2B309, Althanstrasse 14, A-1090 Vienna, Austria
9 Department of Geosciences, University of Oslo, P.O. box 1047, Blindern, N-0316 Oslo, Norway
10 New Mexico Museum of Natural History & Science, Albuquerque, New Mexico 87104, USA
11 Geology Department, SUNY Cortland, Bowers Hall, P.O. Box 2000, Cortland, NY, USA
12 Dept. of Earth & Planetary Sciences, Kyushu Univ.,744 Motooka, Nishi-ku, Fukuoka 819-0395, Japan
13 MTA-MTM-ELTE, Research Group for Paleontology, P. O. Box 137 H-1431, Budapest, Hungary
14 CASP, Madingley Road, Cambridge, UK.
15 Lithosphere and Biosphere Science, Lund University,Box 117, SE-221 00,Lund, Sweden
16 Dipartimento di Geoscienze, Università degli Studi di Padova,Via Gradenigo, 6, I-35131 Padova,Italy
17 GeoZentrum Nordbayern, Universität Erlangen-Nürnberg, Schlossgarten 5, 91054 Erlangen, Germany
18 Department of Geosciences, North Dakota State University, Dept. 2745, Fargo, ND 58108-6050, USA
19 Hacettepe University, Department of Geol.l Engineering, 06800 Beytepe-Ankara,Turkey
20 Nanjing Institute of Geology and Palaeontology, China
21. Faculty of Geosciences, University of Bremen, Klagenfurter Street 2-4, 28359 Bremen, Germany
22 Department of Earth and Atmospheric Sciences, University of Alberta, Edmonton, Canada

Abstract

The Norian Stage is the longest stage in the Phanerozoic, and some members of the boundary working group have been evaluating suitable Carnian-Norian boundary sections for roughly two decades. This has identified two possible candidate boundary sections, at Black Bear Ridge (British Columbia, Canada) and Pizzo Mondello (Sicily, Italy). After a formal voting procedure within the working group, ending on the 26th July, 2021, the Pizzo Mondello section was selected as the global stratotype section and point for the base of the Norian. We evaluated the global correlation potential of the two proposed primary markers, the conodont *Metapolygnathus parvus* and the 'flat-clam' *Halobia austriaca.* Secondary markers were also evaluated around these boundary datums for correlation potential, and the veracity of the proposed sections for GSSP status. Data and arguments for the proposed sections and datums are presented here. Through a two-stage process of option elimination in voting, conforming with ICS guidelines, the working group decided by 60% majority to propose that the first occurrence datum of *Halobia austriaca* in the Pizzo Mondello section

at the base of bed FNP135A should become the 'golden spike' for the base of the Norian. A secondary biotic marker for this boundary is the first occurrence of *Primatella* (*Carnepigondolella*) *gulloae*, in sample NA43, ca. 0 m below FNP135A, and the FA of *Dimorphites noricus* (sample NA42.1) ca. 3.5 m above bed FNP135 (indicating the first subzone of the Jandianus Zone). The best physical secondary marker is the magnetozone PM5n with the proposed boundary ca.40% through the thickness of PM5n. Strengths of the chosen datum are: 1) it also maintains historical priority for ammonoid zonations, which had placed the base Norian near to this level in Europe, North America and probably NE Asia; 2) *Halobia austriaca* is widely distributed in all paleolatitudes and is a long-established taxon.

1. INTRODUCTION

The Norian is a long established late Triassic stage, with the pioneering work of Mojsisovics (1869) indicating a type area in the Hallstatt region of Austria. The underlying late Carnian (Tuvalian Substage) has a type area near the German- Austria border in the Tuval Mountains between Hallein and Berchtesgaden (Lucas, 2010). These divisions were historically defined by ammonoid zonations. The Norian (Late Triassic) is the longest stage in the Phanerozoic and deservedly should have a defined global stratotype and point (GSSP) for its base. This is what the Carnian-Norian boundary (CNB) working group was tasked to decide. Here we present the key arguments proposed for coming to a decision about the choice of the base Norian GSSP. The real process of coming to a final decision started in mid-2020, after decades of effort focused on the two candidates at Black Bear Ridge (BBR) in British Columbia, Canada and Pizzo Mondello (PM) in Sicily, Italy (but also at other sections). This work details the data and arguments leading the group towards a decision, which will be later formally submitted to the Subcommission on Triassic Stratigraphy (STS). For the sake of transparency, this article outlines the decision processes and key outcomes that led to the final choice.

Section 1 is a summary of the key attributes of the two candidate sections and an evaluation of the accessibility and protection of both BBR and PM. Sections 2 and 3 examine the cases for global correlation using the two primary markers (datums) previously proposed. These are the first occurrence (FO) *Metapolygnathus parvus* datum detailed in section 2 and the FO of *Halobia austriaca* detailed in section 3. These cases also consider the use of possible secondary markers to enhance the correlation potential.

Section 4 examines other correlation issues beyond the proposed primary markers. Specifically, correlation into high palaeolatitude sections (section 4.1), use of radiolarian zonations (section 4.2), isotopic changes across the boundary (section 4.3), the nature of possible condensed or hiatal intervals at BBR (section 4.4), and the strengths of historical priority if using FAD of *H. austriaca* (section 4.5). Section 5 details the outcome of the formal voting within the working group.

Inevitable there remain some divergences in interpretation of datasets and taxonomic divisions. These divergences are presented together in places in the text to express both sides of the arguments presented. Contributors to particular parts of the text are indicated at section ends to display in part this divergence of views.

1. SUMMARY OF QUALIFICATIONS OF THE BLACK BEAR RIDGE AND PIZZO MONELLO SECTIONS

1.1 Accessibility and protection of the section at Black Bear Ridge

The Black Bear Ridge section is on the north shore of the Peace Reach of Williston Lake, 3.7 kilometres northeast of the mouth of the Nabesche River. Williston Lake was created in 1967 by the damming of the Peace River. There is good exposure (Figs. 1, 2) due to periodic lake level changes that clean the shore surface. The section contains a complete section through the Late Triassic into the Hettangian.

Black Bear Ridge meets all geological requirements for a GSSP (Table 1). Black Bear Ridge includes several hundred metres of section, preserving a continuous record from the Carnian (*samueli* Zone) through to the latest Norian (*bidentata* Zone). Further outcrop occurs in the Rhaetian and Hettangian, but an erosional unconformity is present at the Norian-Rhaetian boundary. This unconformity is several hundred metres above the GSSP candidate horizon and post-dates it by approximately 19 million years.

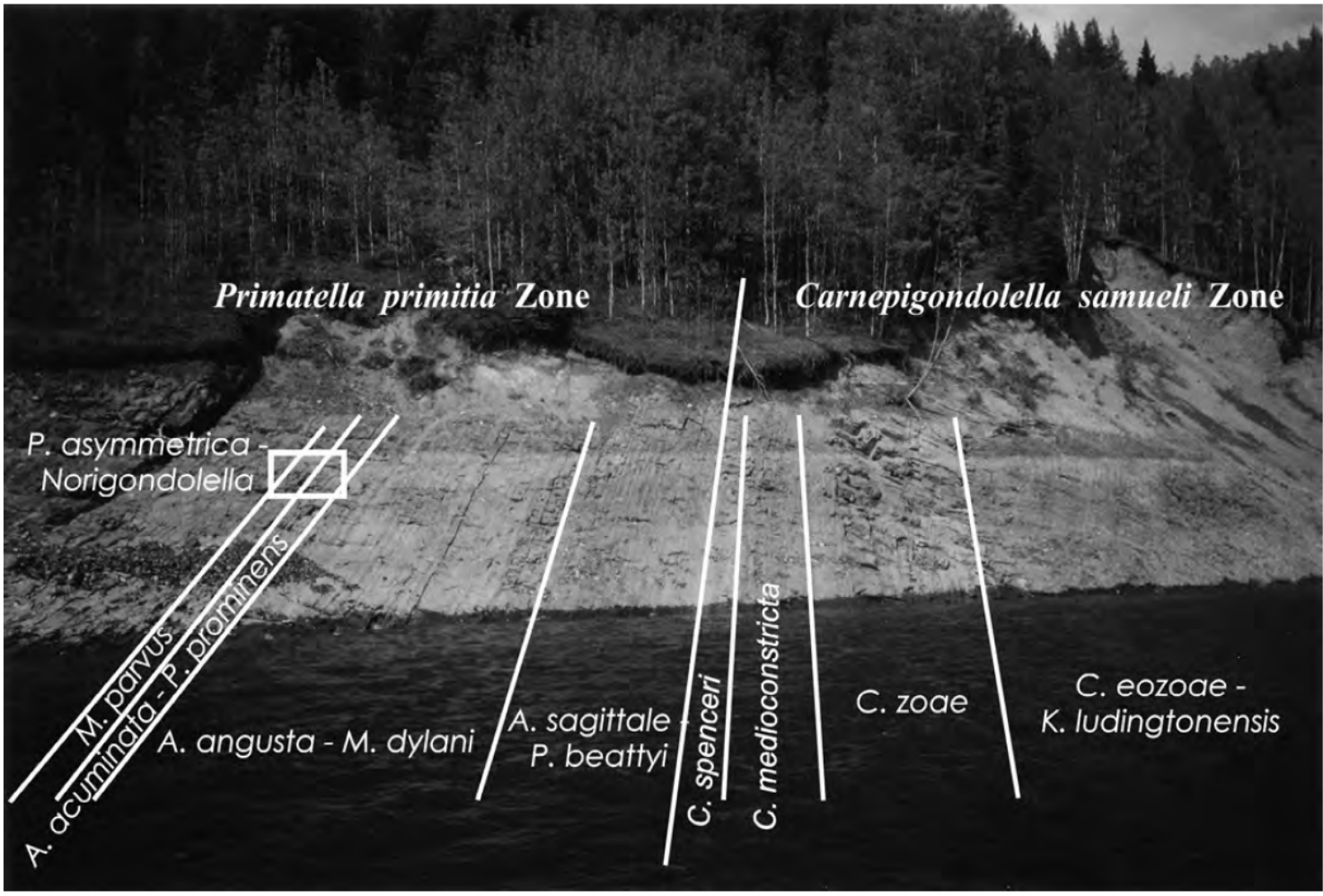

Fig. 1. Conodont zonation placed onto on the BBR section (Orchard, 2014). Fig. 2 shows the inset-square in detail.

The Carnian-Norian boundary interval is characterized by a single lithofacies, strong evidence of continuous sedimentation through the boundary interval, and is devoid of evidence of synsedimentary or tectonic disturbance or evidence of metamorphism/strong

diagenetic alteration. The Black Bear ridge section could be considered mildly condensed, in that sedimentation rates were low and the CNB interval (here defined as the interval from several metres below the oldest datum under consideration to several metres above the highest datum being considered) is approximately 25 metres in vertical thickness.

The Carnian-Norian boundary interval at Black Bear Ridge consists of a single facies succession deposited in a quiescent deep marine basin that was well below storm wave base and that was not affected by deep marine currents. Black Bear Ridge has an exceptional fossil record with well-preserved conodonts and bivalves as well as several horizons that produce well-preserved ammonoids (Figs. 1,2; Table 1).

It is the conodont record that renders Black Bear Ridge exceptional, with continuous conodont production throughout the entire interval. Conodont samples are diverse, abundant and very well preserved. The conodont fauna includes multiple evolutionary lineages and preserves clear morphological clines within lineages. Many collections produce hundreds of conodonts per kilogram. Similarly, the horizons with *Halobia,* including those with *H. austriaca,* are characterized by abundant specimens as well.

The conodont taxonomy and zonation developed around the CNB at BBR, and nearby locations in northeast British Columbia, has been successfully applied in lower paleolatitude Nevada (Balini et al., 2015), in the Panthalassan terrane of Wrangellia (Carter & Orchard, 2013), and recently in far flung Timor (work in prep.). This demonstrates the wide distribution of BBR conodont taxa, and the latter study provides correlation with the Oceanic realm via the Haida Gwaii radiolarian succession that is fully integrated with BBR conodont zones (Section 4.3).

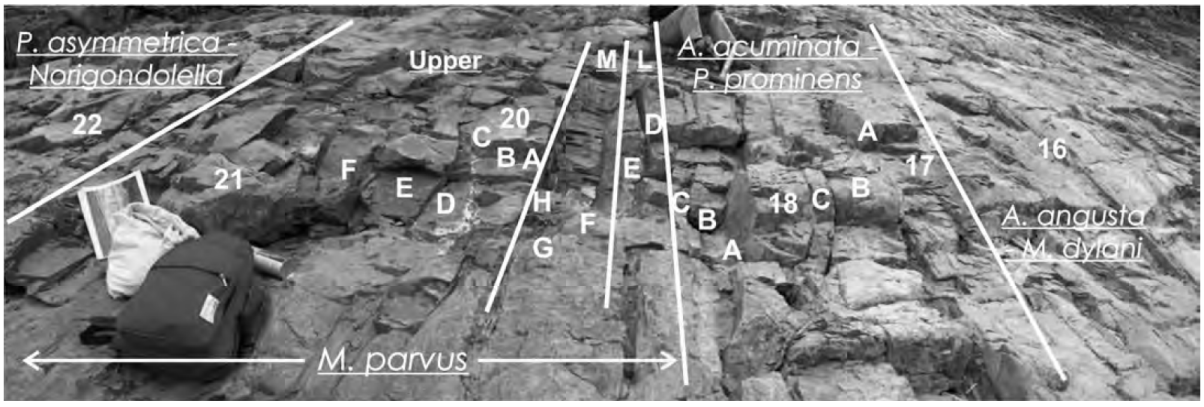

Fig. 2. Detailed conodont zonation in the critical *parvus* Zone interval at BBR (From Orchard, 2014). The FO of *Halobia austriaca* is in bed 22.

Site Access: The nearest regional airport to Black Bear Ridge is located in Fort St. John, which is accessible via direct flights from Calgary, Edmonton and Vancouver. The site is accessed via a 90-minute drive from Fort St. John to Dunlevy boat launch east of the hamlet of Hudson Hope. From the boat launch, Black Bear Ridge is a 48 km boat ride up the Peace Reach of Williston Lake. Boat hire is simple and economic, and researchers can be dropped off on a beach 50 metres from the boundary interval. Alternatively, the site can be accessed by chartering a flight from Fort St. John to the Ottertail Landing Strip, which can handle small and medium-sized planes (up to Twin-Otter). This landing strip is 3.9 km from Black Bear Ridge and is connected to a functional but disused logging road that enters the valley on the west flank of Black Bear Ridge, 300 metres from the outcrop section.

Protection: Outcrop exposure at Black Bear Ridge occur on the southern flank of a tree-covered ridge in the southern Muskwa Range. Black Bear Ridge is located on British

Columbia Crown Land. This land is designated as multiuse land, on which activities such as forestry (logging), hunting, trapping and geological research are allowed. The area is also part of a hunting and guiding lease area currently held by Williston Lake Outfitters.

The entirety of Black Bear Ridge and the hills and ridges adjacent to it, consist of Jurassic and Triassic strata of the Ludington, Pardonet and Fernie formations. None of these contain economically important minerals or rocks, so mining is not a concern in this area. Black Bear Ridge is secure from development or alteration as it currently stands. Black Bear Ridge is not, at present, located within a provincial park or a national park. Obtaining further provincial protection for this locality can easily be accomplished but is not necessary. Under present rules no further development is permitted in this area. Regardless, should Black Bear Ridge be chosen as the base Norian GSSP, we will initiate the necessary steps to attain the equal protection that making this an official provincial protected area would afford.

(Zonneveld, Orchard)

Data Type	**Details**
Conodonts	A detailed zonation at ~15 cm precision. See Orchard (2007; 2014, 2019) and Section 2.
Halobia	See McRoberts (in press) and McRoberts (2007, 2010).
Ammonoids	Ammonoid recovery sporadic. Supplemented by direct (from matrix) calibration to conodont zonation from wider B.C area (fig. 5 in Orchard, 2019). Details in Orchard (2014, 2019), Balini et al. (2012) and Fig. 13.
Radiolaria	Not within the section, but calibrated to conodont zonation from Haida Gwaii sections. See Carter & Orchard (2013) and Section 4.3.
Palynology	None available
Nannofossils	None available
Foraminifera	None available
Magnetostratigraphy	None: Remagnetised in the Upper Cretaceous (Muttoni et al., 2001b)
Carbonate carbon isotope stratigraphy	An excursion, or excursions are evident, but ability to correlate these has not been fully tested (Section 4.4). Detailed sampling within the *parvus* Zone (Onoue et al., 2016), and also wider within the section (Lei et al. 2021).
Organic carbon isotope stratigraphy	cm-scale record from Williford et al. (2007) through the lower and mid part of the Parvus Zone, much wider outside this interval (Fig. 10).
Sr-Isotope stratigraphy	Within the 7 m interval through the boundary interval, $^{87}Sr/^{86}Sr$ declining from ca. 0.7082 to 0.7080 at base and top of Parvus Zone respectively (Onoue et al., 2016).
Oxygen-Isotope stratigraphy	Based on conodont phosphate, at ~50 cm spacing providing temperature estimates (Sun et al. 2020)
Cyclostratigraphy	None available, but a study may be possible.
Radiometric dating	None available, but possible using correlation to study of Mietto et al (2021).
Sequence stratigraphy/ sedimentology	Zonneveld et al. (2010). The CNB boundary interval is predominantly calcareous turbidites with lesser hemipelagic suspension deposits. Boundary interval with a succession showing progressive sea-level rise.
Other data	ichthyoliths: Orchard et al. (2001)
Thermal maturity/tectonics	CAI = ~3, Black Bear Ridge occurs on the Pardonet Hill Thrust sheet (text-fig. 1), on the eastern margin of the Nabesche Syncline. Beds dip 75°. Although minor bedding plane slippage has occurred above the

	study interval during thrusting, fault repetition does not occur within the study interval (Riediger et al. 2004).
Nearby sections	Juvavites Cove (~3km south), Pardonet Hill East (~2 Km south-southeast), Brown Hill, West Schooler Creek, East Carbon Creek, and McLay Spur.

Table 1. Summary of the key stratigraphic attributes of the Black Bear Ridge section

1.2 Accessibility and Protection of the section at Pizzo Mondello

The section is part of the 430 m thick Scillato Formation (also known as ‘‘cherty limestone’’ or ‘‘Calcari con selce’’ or Halobia Limestone in Sicily). The Pizzo Mondello section (about 600 a.s.l.) is in an abandoned quarry in the lowermost part of the SW slope of Pizzo Mondello, about 3 km WNW of Bivona village (Fig. 3). Beds are well exposed and can be followed along strike for about 400 meters. The Pizzo Mondello section meets all geological requirements for a GSSP (Table 2).

The Pizzo Mondello section can be visited from January to December. The easiest access is from Palermo International Airport ‘Falcone e Borsellino’, well served by several car rental agencies. Bivona is 120 km from the airport, which take about two-and-a-half hours by car. The route is by the freeway E90 until Villabate, then by SS121 until Lercara Friddi, then by SS188 and SS118. The site can be reached from Bivona in 15 minutes by paved road (SP34) and dirt road, and then 5 minutes walking across peach orchards.

Fig. 3. Pizzo Mondello section B (see Nicora et al. 2007), with the position of some key bioevents and of the two GSSP datum options. The section has been measured and sampled along three partially overlapping segments (yellow dashed lines).

The Pizzo Mondello section is located in a wide area that is owned by the Municipality of Bivona.

The Pizzo Mondello section is under strict protection rules, because it is included in the protected area 'Riserva Naturale Orientata Monti di Palazzo Adriano e Valle del Sosio'. This protected area is included also in the European Commission (EC) protected areas network Natura 2000, Habitat' as 'SIC Monte Rose and Monte Pernice' (code ITA020029). This area is registered by the Italian Ministry of Environment as a Special Zone of Conservation. Protection rules include strong restrictions on any anthropogenic activities but unlimited and free access for scientific studies.

A project for the development of the protected area 'SIC Monte Rose and Monte Pernice' has been granted funding by the EC. This project includes improvement of accessibility to the Pizzo Mondello section and preparation of explanatory panels for guided tours. The improved accessibility will allow visits to the Pizzo Mondello section by disabled visitors.

The site of the GSSP candidate is included in the list proposed as a Geosite of global importance (code NAT-1BI-0037) by the Regional Government of Sicily (Figs. 4, 5). In case of selection as the GSSP, Pizzo Mondello will also be included in the list of the GSSP Geosites by the Italian Geological Survey (Serviio Geologico d'Italia, ISPRA).

(Balini, Nicora, Rigo)

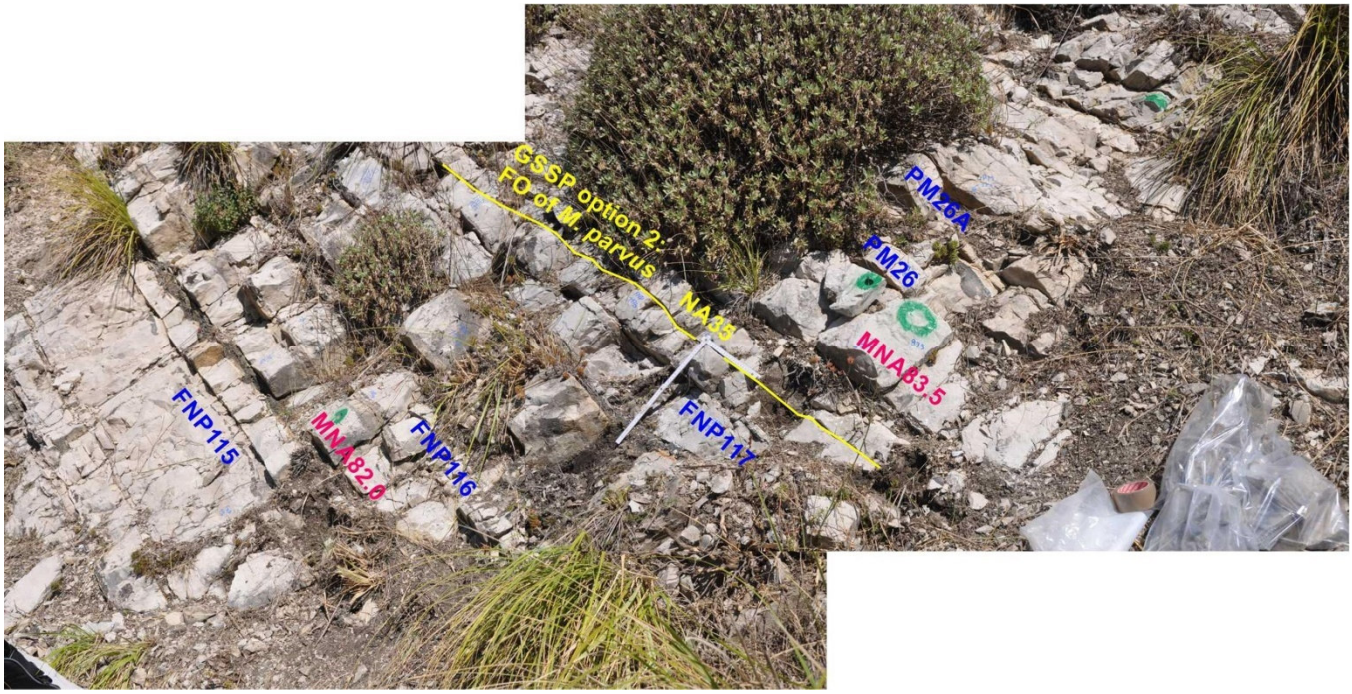

Fig. 4 The interval including the bed NA35, recording the FO of *Metapolygnathus parvus*. In purple, the paleomagnetic samples MNA82.0 (87.5 m from the base) and MNA83.5 (89 m from the base). Only the most important samples are shown in the picture.

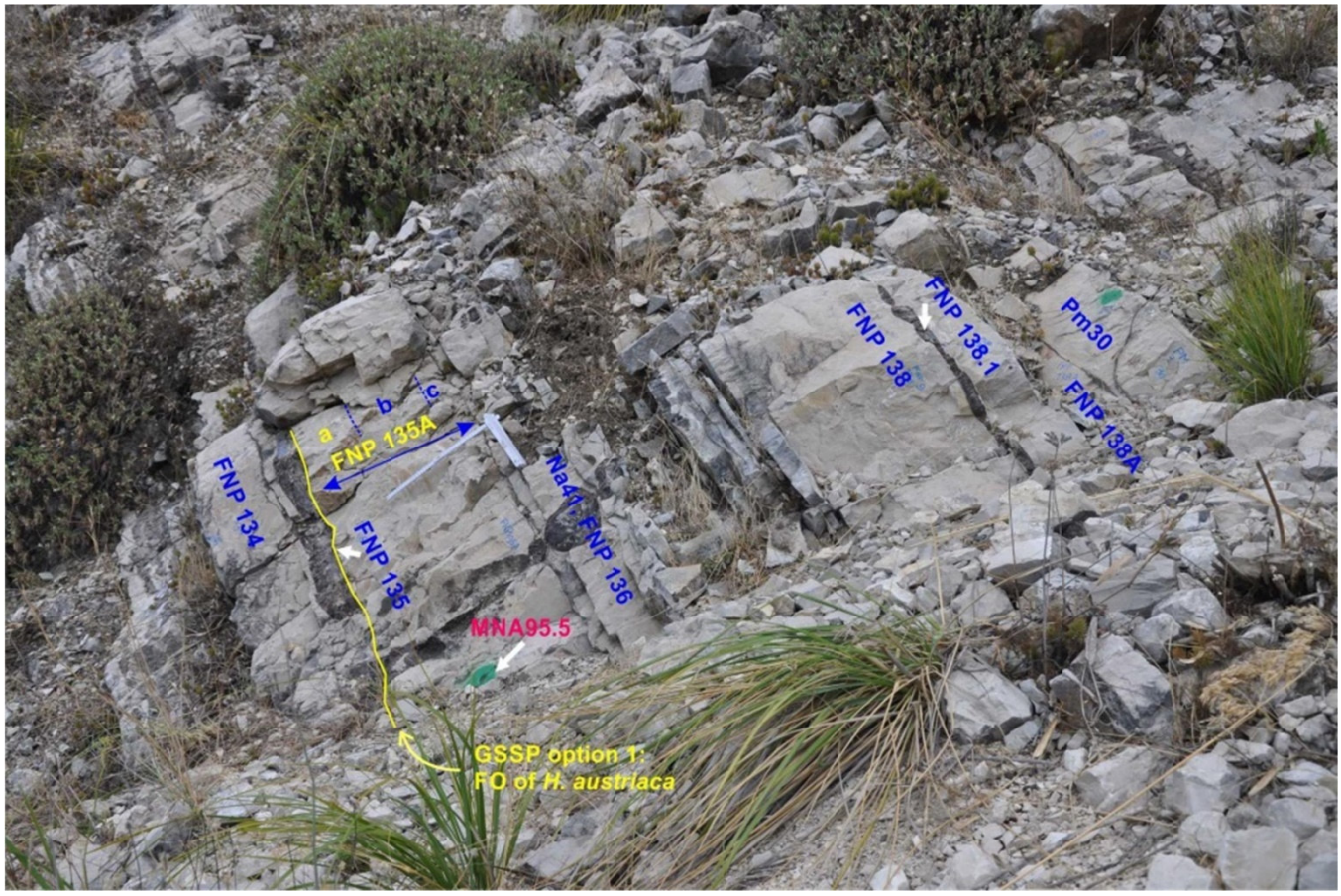

Fig. 5 Pizzo Mondello interval including the bed FNP135A, recording the FAD of *Halobia austriaca*. The bed FNP135A is 55-60 cm thick, for a more accurate location of the FO of *H. austriaca*, starting from 2012, the sampling of this bed has been done by subdividing it in three portions: a, b and c. The FAD of *H. austriaca* is recorded at the base of FNP135Aa. Paleomagnetic sample MNA95.5 (101 m from the base of the section) is in the middle of FNP135A. Only the most important samples are shown in the picture.

Data Type	**Details**
Conodonts	A zonation at ~1 m precision over the CNB boundary interval (Mazza et al. 2010, 2012a, 2018). Figs. 3, 18.
Halobia	A detailed Halobiid zonation with recovery at ~0.5 m spacing (Levera, 2012). Fig. 7, 19.
Ammonoids	Around 130 ammonoids from around 100 m of section, mostly 1 per bed, sometimes more. See Balini et al. (2012) for detail and Fig. 11
Radiolaria	Common and well preserved (Nicora et al, 2007; Guaiumi, 2008, Balini et al., 2008), but not published in detail.
Palynology	None available from the section, but within the area is a study by Visscher and Krystyn (1978).
Nannofossils	Bellanca et al. (1995); Preto et al. (2013), but no detail over CNB interval
Foraminifera	Preto et al (2013), but no detail published over CNB interval
Magnetostratigraphy	Good magnetostratigraphy allowing global correlation through late Carnian to Rhaetian interval (Muttoni et al. 2001a,2004). Sample spacing ~1.2 m, but more detailed in some intervals outside CNB.
Carbonate carbon isotope stratigraphy	Whole-rock $\delta^{13}C$ sampling at ~2 m, Muttoni et al. (2014) and more detailed micro-drill sampling by Mazza et al. (2010). Shift to positive

	values at around the middle of the Parvus Zone (Fig. 4).
Organic carbon isotope stratigraphy	None available
Sr-Isotope stratigraphy	Sampling at ~ 2 m spacing over the CNB (Onoue et al. 2018). $^{87}Sr/^{86}Sr$ declining slightly from ca. 0.7077 through the Parvus Zone respectively (Onoue et al., 2018).
oxygen-Isotope stratigraphy	Sampling at ~ 4 m spacing over the CNB (Rigo et al. 2012b).
Cyclostratigraphy	Available for the Norian (Hüsing et al., 2011). May be possible for the boundary interval (see Fig. 17). Magnetostratigraphy allows correlation to Newark Supergroup cyclostratigraphy (Kent et al., 2017).
Radiometric dating	None available, but possible using correlation to study of Mietto et al (2021).
Sequence stratigraphy/ sedimentology	Lithologically, the succession consists mostly of evenly bedded to nodular *Halobia*-bearing cherty calcilutites (Guaiumi, 2008). Sequence stratigraphy: none available.
Thermal maturity/tectonics	CAI=1, maximum burial temperature <50-80^{o}C (Guaiumi, 2008). The section is located in the lowermost Sicanian thrust sheet (Pizzo Mondello tectonic unit) that overthursts upper Tortonian-Messinian clays, consists of three Triassic units, the Mufara Formation, the Scillato Formation and the Portella Gebbia Limestone.
Nearby sections	A number of other sections in the area at Monte Triona and Monte Cammarata. Balini et al. discussed these sections during STRATI 2019.

Table 2. Summary of the key stratigraphic data attributes of the Pizzo Mondello section.

2. KEY ATTRIBUTES OF THE CONODONT *METAPOLYGNATHUS PARVUS* AS THE PRIMARY MARKER TO DEFINE THE BASE OF THE NORIAN

It is probable that the FAD of *Metapolygnathus parvus* (Fig. 6) is the best primary marker to define the base of the Norian Stage. *Metapolygnathus parvus* is in fact, the most reliable and useful biomarker because this species is morphologically simple and easy to recognise, and its FO is globally recognisable within a clear phylogenetic lineage (Figs. 6, 7A, 7B).

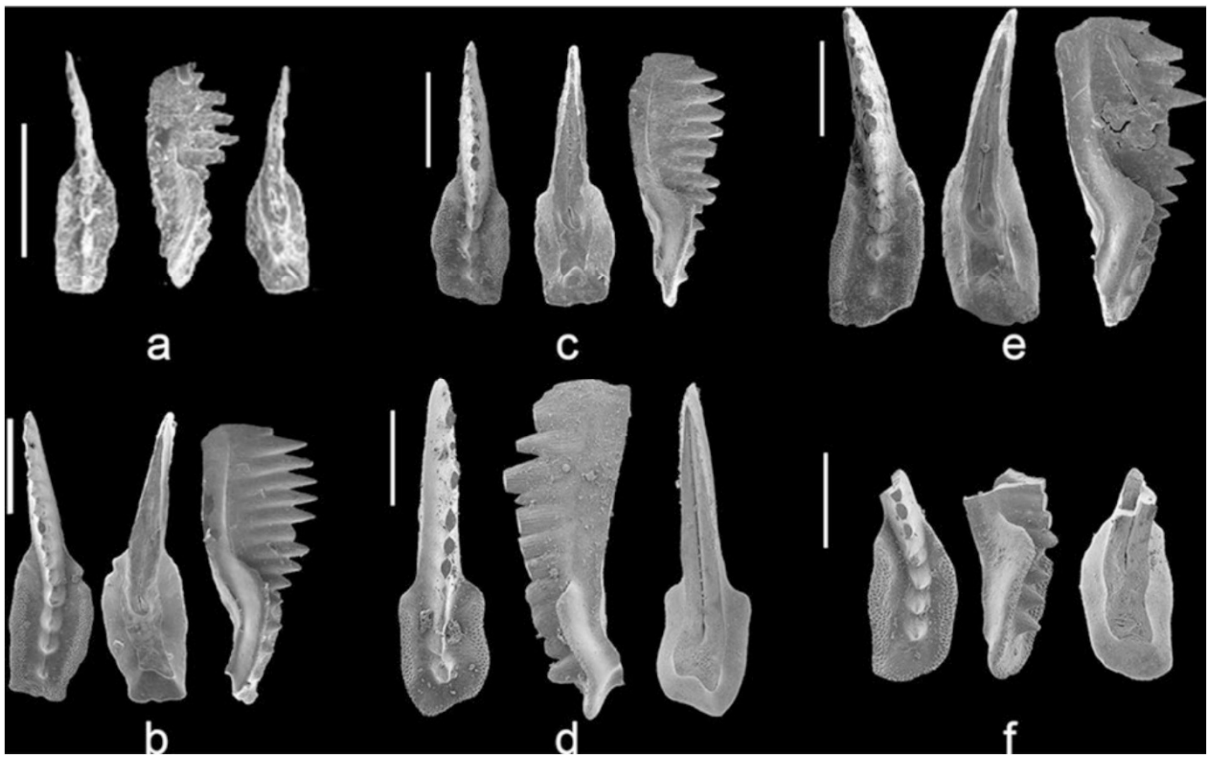

Fig. 6. This figure is fig. 6.11 in Rigo et al. (2018) where species of *Metapolygnathus parvus* Kozur are illustrated (the α morphotype *sensu* Orchard, 2014) from locations in: (a) The northern Tethys (from Noyan & Kozur 2007, their fig. 7.1). (b) The Neotethys (from Mazza & Martínez-Pérez 2016, Pl. 6, fig. 24). (c) Neotethys (from Mazza & Martínez-Pérez 2015, Pl. 6, fig. 23). (d) North America, from Orchard 2014, fig. 48, 14–16; (e) Neotethys (from Mazza & Martínez-Pérez 2016, Pl. 6, fig. 25). (f) North America (from Orchard 2014, fig. 48, 17–19). Scale bars are 200 µm.

Overview: Outside of the Triassic, some 23 stage bases are defined by conodont primary markers, with most of these in the Devonian-Carboniferous-Permian, indicating the widely accepted suitability of conodonts for GSSP definition. There is also an incredible level of detail published on the biostratigraphy and phylogenesis of Upper Triassic conodonts, indicating that conodont bioevents may provide the detail to make them the preferred markers for defining stage boundaries, such as the Carnian-Norian boundary (Nicora et al., 2007; Orchard, 2007, 2010, 2014, 2019; Balini et al., 2010; Rigo et al., 2018; Mazza et al., 2018). The conodont work has provided a great range of knowledge of conodont biostratigraphy across the Carnian-Norian boundary, in both GSSP candidate sections

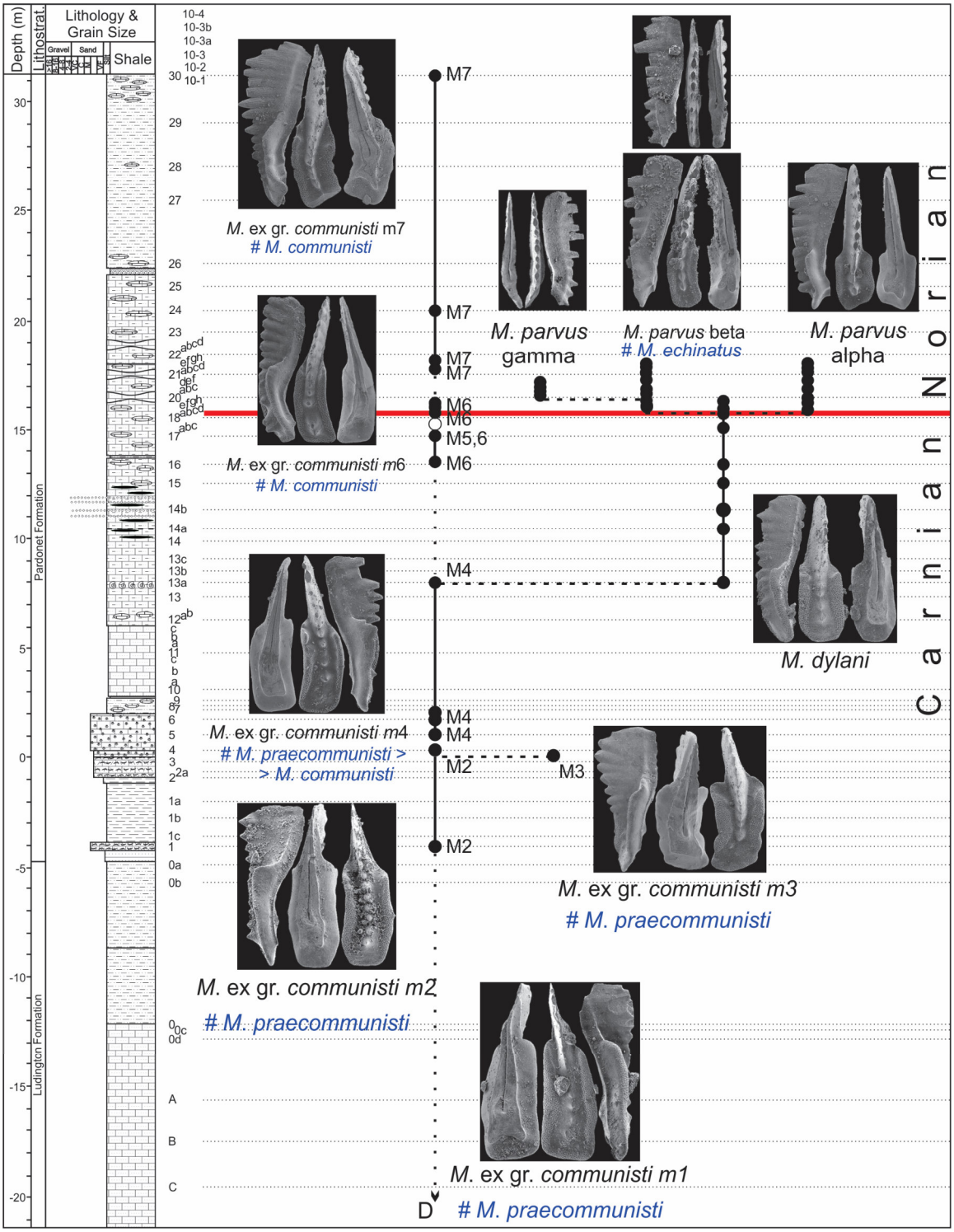

Fig. 7A. Evolution and proposed phylogenetic relationships of *M.* ex. gr. *communisti*, *M. dylani* and *M. parvus* at Black Bear Ridge (modified from fig. 13 of Orchard, 2014). Names after # (and in blue) are those used by Mazza et al. (2018) for these forms.

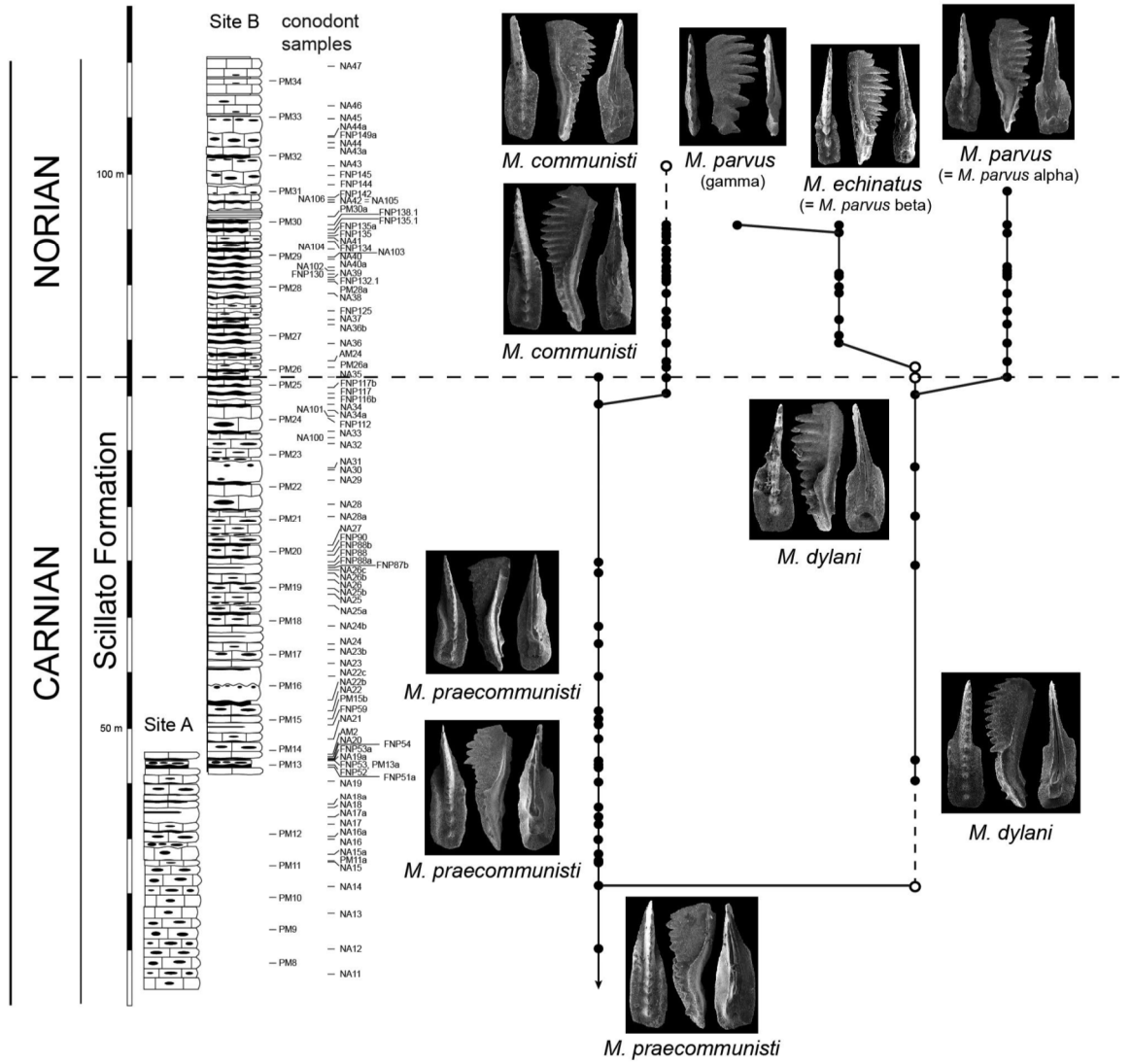

Fig. 7B. From Mazza et al. (2018). Evolution and phylogenetic relationships of *Metapolygnathus praecommunisti* Mazza, et al. (2012a), *M. communisti* Hayashi, 1968, *M. dylani* Orchard, 2014, and *M. parvus* Kozur, 1972 at the Pizzo Mondello section. The figure is drawn based on the model of fig. 13 of Orchard (2014) for a better comparison between the conodont ranges and evolution in the two sections. Empty circles in the *M. dylani* range indicate transitional forms, while empty circle in the *M. communisti* range refers to *M.* cf. communisti. Conodonts are not to scale.

of the Norian Stage base, at Pizzo Mondello (Mutoni et al., 2001a; Nicora et al., 2007; Balini et al., 2010; Mazza et al., 2010, 2011, 2012a, b; Mazza & Martínez-Pérez, 2015) and Black Bear Ridge (Orchard et al., 2001b; McRoberts, 2007; Orchard, 2007, 2014, 2019; Balini et al., 2015). From both the Pizzo Mondello section and Black Bear Ridge section (BBR), conodonts were first described 20 years ago (Muttoni et al., 2001a; Orchard et al., 2001b).

One of the factors that has contributed to wide use of conodonts for GSSP definition is that meter to cm details of stratigraphic distribution is only limited by the density of sampling (provided conodonts are present), something that is generally not possible with macrofossils, which often have a sporadic stratigraphic distribution, particularly in the Late Triassic (Balini et al., 2012).

Evolutionary trends: In the Late Triassic, conodonts suffered four main extinction events before the end of the Rhaetian, probably related to climatic changes (Trotter et al., 2015; Sun et al., 2020): 1) in the early Julian; 2) near the Julian/Tuvalian substage boundary (mid-Carnian); 3) near the Carnian/Norian boundary; and b) near the Norian/Rhaetian boundary. After the extinction at the Julian/Tuvalian boundary, slow recovery brought conodont diversity to a new peak in the middle to late Tuvalian, e.g. the rise of the genera *Carnepigondolella*, *Kraussodontus, Metapolygnathus*, *Norigondolella*, *Parapatella*, *Primatella* and *Quadralella* (e.g. Mazza et al., 2010, 2018; Orchard, 2014, 2019). In eastern Panthalassa, *Acuminatella* is also widespread (Carter & Orchard, 2013; Balini et al., 2015). Faunal turnover at the Carnian-Norian boundary was characterized by a dramatic drop in diversity as several of these conodont stocks disappeared (Figs. 7A, 7B; Mazza et al., 2010; Orchard 2014). Far fewer new taxa appear in the CNB interval; notable amongst these is the short-lived *Metapolygnathus parvus* and similar diminutive elements (Orchard, 2014). Younger Norian faunas at BBR contain only ornate *Acuminatella* and *Primatella* and occasional floods of cool water *Norigondolella* (Trotter et al., 2015; Sun et al., 2020).

At Pizzo Mondello, three conodont faunal turnovers, named T1, T2, and T3, have been identified (Mazza et al., 2010) and correlated between PM and BBR (Mazza et al., 2018; Orchard, 2019; Fig. 8). T2 is characterized by the mass development and expansion of the genus *Metapolygnathus* and the demise of typical Carnian taxa (Mazza et al., 2018). The T2 turnover event is placed at the base of the *Metapolygnathus parvus* Zone at PM, which corresponds to the base of the *Metapolygnathus parvus* Subzone (mid *Primitella primitia* Zone) at BBR. The appearance of the index species *M. parvus* is the key datum common to both sections, together with the appearance of other morphotypes (Figs. 7A, 7B). Their similarity in development refutes the impression of strong provincial differences.

Origin of *Metapolygnathus parvus:* During the late Tuvalian, several lineages of conodonts exhibited a reduction in platform size (that is the length of the platform relative to that of the blade) and an anterior migration of the pit (e.g. Mazza et al., 2018; Orchard, 2007, 2014, 2019). This is particularly true in *Metapolygnathus* and *Parapatella* (Orchard, 2014). This diminution in *Metapolygnathus* is manifest in the appearance of *M. parvus,* which is an easily recognisable species that descended from *M. dylani* (Orchard, 2014, 2019; Mazza et al., 2018; Figs. 7A, 7B). This phylogenetic lineage is well documented in both candidate GSSP sections.

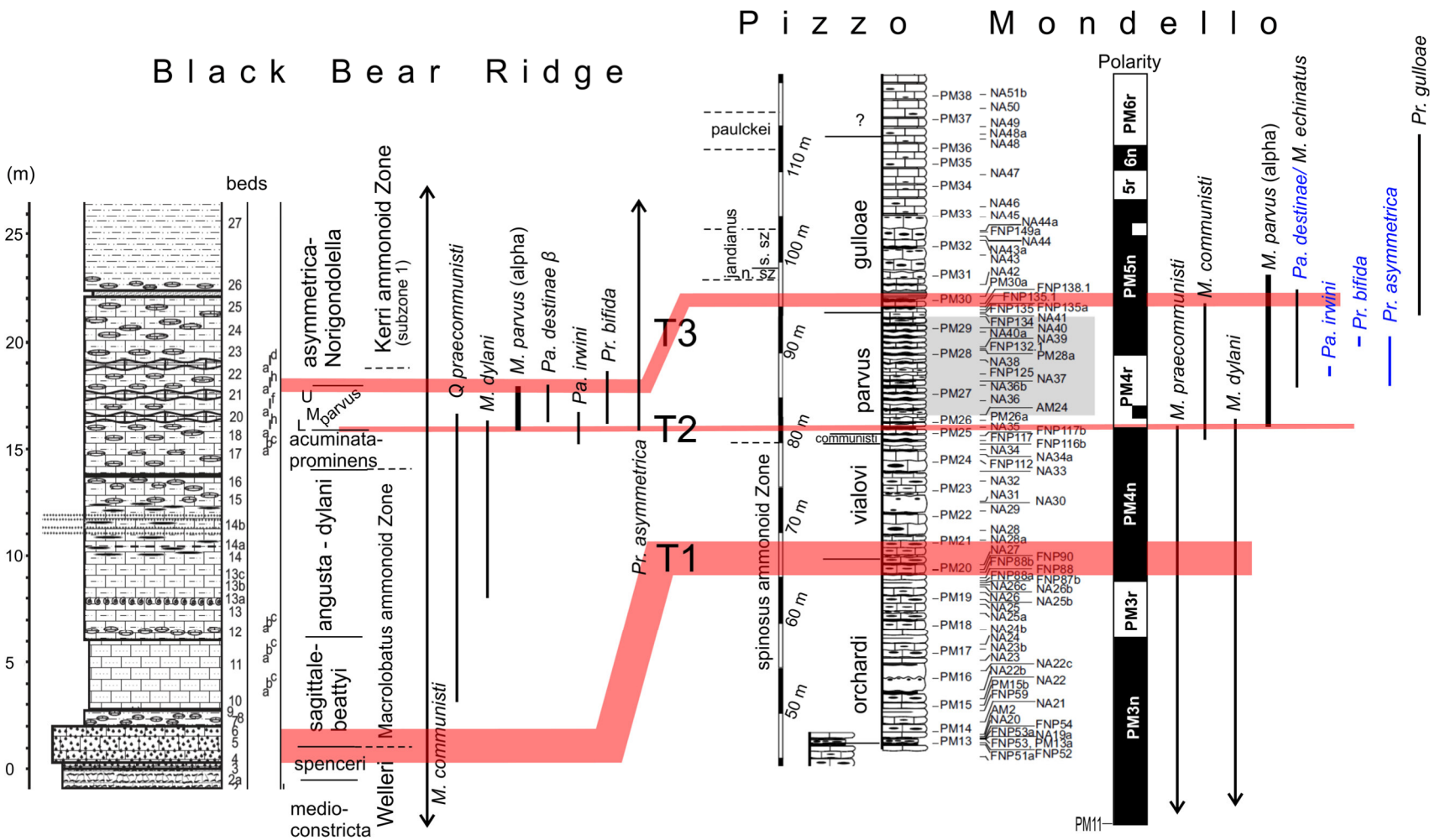

Fig. 8. Correlation between BBR and PM (based on Mazza et al. 2012a; 2018; Orchard, 2019), using the conodont turnovers T1 to T3, and some conodont other taxa (M. = Metapolygnathus, Pa. = Parapetella, Pr. = Primatella, Q.= Quadralella), selected to show the similarity in faunas in the *M. parvus* Subzone/Zone in the two sections (those in blue based on Orchard's (2019) evaluation of between-section similarities, based on published illustrations only). Magnetostratigraphic data (magnetozones PM3n to PM6r) from Muttoni et al. (2004), with palaeomagnetic sampling positions (PM13 to PM38) matched to the height scale. Divergent views remain on the β morphotype of *M. parvus* with *Pa. destinae* and *M. echinatus* shown.

The conodont *Metapolygnathus parvus* was established by Kozur in 1972 from the section at Silická Brezová (Slovakia), but the illustrated holotype belonged to a juvenile specimen (as noted by Krystyn, 1980) and not to an adult individual of *Me. parvus*. After more than 30 years, the criticisms of *Me. parvus* were addressed by Noyan & Kozur (2007), admitting that the holotype was established from a rich fauna consisting exclusively of juvenile forms of this species, but indicating that adult faunas are also abundant (Noyan & Kozur, 2007, p. 171). Noyan & Kozur (2007) also presented a detailed analysis of the *Metapolygnathus communisti* group, based on new material from the Stefanion section (Argolis, Greece), a pelagic succession belonging to the northern shelf of the Pindos-Huğlu Ocean, in northern Tethys (Fig. 6a). These authors described four species and two subspecies belonging to the *communisti* group: *Me. communisti communisti* Noyan & Kozur, 2007*, Me. communisti parvus, Me. multinodosus* Noyan & Kozur, 2007*, Me. linguiformis,* and *Me. angustus* Kozur, 1972. *Metapolygnathus parvus* was thus defined as a subspecies of *Me. communisti* and re-illustrated and re-described as an *M. communisti* with a shorter platform, with a more forward shifted pit and no nodes on the platform margins (Noyan & Kozur, 2007, fig. 7.1, p. 171). Recently, Orchard (2014, 2019) considered instead *Me. parvus* the descendant of the newly established species *Metapolygnathus dylani* Orchard, 2014: "*Metapolygnathus dylani* sp. nov. is interpreted to have evolved from *Me.* ex gr. *communisti* through reduction of the anterior platform and the relative lengthening of the free blade (Figs. 7A, 7B). A continuation of this trend is thought to have led to *Me. parvus*, which has a substantially reduced platform that is less than half of the total element length and an anterior pit" (Orchard, 2014, p. 10). Orchard (2014) also differentiated three morphotypes that showed different degrees of platform development- similar, but not identical morphotypes can also be found at PM (Figs. 7A, 7B, 8). *Metapolygnathus parvus* Kozur is the α morphotype of Orchard (2014).

The phylogenetic lineage and morphological characteristics of *M. parvus* are well established, and widely accepted amongst conodont workers, making this a suitable 'stable' primary marker for the base of the Norian.

Wider Occurrence: *Metapolygnathus parvus* have been collected from different depositional environments, such as periplatform carbonates, distally steepened carbonate ramp/medial to distal slope environments and proximal to deep water pelagic environments, including cherts deposited below the CCD (NE China), and at different paleolatitudes on both sides of Pangea. *Me. parvus* is reported to occur in North America at Black Bear Ridge, Pardonet Hill, and Juvavites Cove in the autochthonous Western Canada Basin (Orchard, 2014, 2019), and at Huxley Island, Sadler Point, and Frederick Island in the allochthonous Panthalassan Wrangel terrane (Carter & Orchard, 2013). Also, it is present in Tethyan successions, such as at Pizzo Mondello and Pizzo Lupo (Sicily, Italy), the Bölücektasi Tepe and Erenkolu Mezarlik sections (Turkey), the Silická Brezová section (Slovakia) (Mazza & Krystyn, 2015), the Csővár borehole (Hungary) (Mazza & Krystyn, 2015), the Gianni Grieco section, Lagonegro Basin (Southern Apennines, Italy) (Rigo et al., 2012a), Slovenia (Kolar-Jurkovsek, 1982), the Argolis section (Greece) (Noyan & Kozur, 2007). In addition, from the Nakijin Formation in the Hedomisaki area (Okinawa, Japan) (Yamashita et al., 2016); and from the mid-Panthalassa Nadandaha Range (Northeast China) (Buryi, 1996), and Mota Hai Luli, Timor-Leste (Orchard and Rigo, unpublished data). Its widespread presence indicates the suitability of *Me. parvus* for defining the base of the Norian.

Lifestyle: Based on its broad distribution, on its occurrence in proximal to distal to open pelagic marine setting, and on $\delta^{18}O_{phosp}$ analysed directly on *Me. parvus* apatite (Trotter et al., 2015), it is concluded that *Me. parvus* was a surface dweller.

2.2 *Metapolygnathus parvus*: reliability and relationship with physical and biotic events

- The species is easily recognisable.
- It is possible to identify the FAD of *Me. parvus* within the hypothesized lineage *Metapolygnathus* ex gr. *communisti (praecommunisti)- Me. dylani - Me. parvus* in both candidate GSSP sections (Pizzo Mondello and Black Bear Ridge).
- *Me. parvus* is documented to occur homotaxially at the base of the evolutionary morphological turnover T2, both at Pizzo Mondello (Tethys) and within the *Me. primitius* Zone at Black Bear Ridge (North America).
- It is coincident with a diminution in some conodont stocks, and the disappearance of many more typically Carnian conodonts in both candidate sections. This also coincides with the mass occurrence of evolutionary advanced metapolygnathids at PM, and a flourish of comparable elements assigned to *Parapatella* and *Quadralella* at BBR (and at PM; as assigned by Orchard, 2019; Fig. 8). The range of *Me. parvus* thus marks a turnover between typically Carnian to Norian species, completed by the time of the last occurrence of *Me. parvus*.
- Its first appearance is below the first occurrence of *Halobia austriaca* in both candidate sections, and also at Silická Brezova and Erenkolu Mezarlik (Krystyn & Gallet, 2002).
- It occurs in different marine depositional environments, such as periplatform carbonates, distal ramp/slope, and from bedded cherts deposited below the CCD.

2.3 Potential secondary markers for the base Norian near the FAD of *Me. parvus*

Correlation to other sections without conodonts would be based on associated secondary markers (Table 3):

- At both GSSP candidates, the range of *Me. parvus* is placed between Upper Carnian strata with the ammonoid *Anatropites* and Lower Norian strata with *Guembelites* in North America and *Dimorphites* in the Tethys. The proposed boundary in the candidate sections therefore falls in the 'traditional Carnian-Norian' transition interval. The FO of *Me. parvus* also occurs just prior to *Pterosirenites* cf. *auritus* at BBR (in bed 18D; Fig. 2), an ammonoid species typical of what has been inferred to be earliest Norian (Kinasovi Zone) in the Boreal realm (Konstantinov et al., 2003; Konstantinov, 2019; Balini et al., 2012). The base of the Kinasovi Zone may therefore provide a secondary proxy for the base of the Norian in Boreal sections.

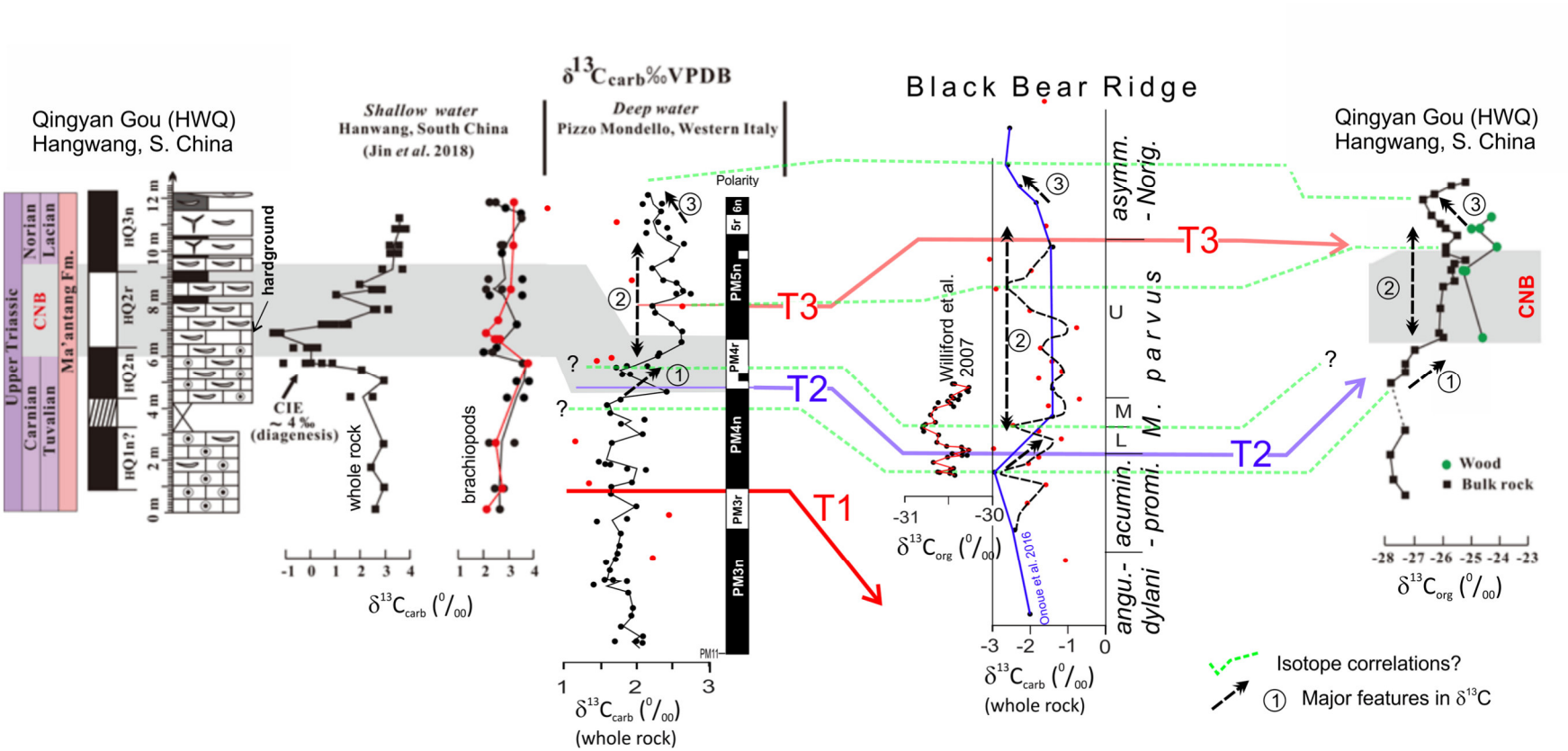

Fig. 9. Carbon isotope data across the Carnian-Norian boundary. Partly based on fig. 11a in Jin et al. (2019), but re-drawn. Carbon isotope data for Pizzo Mondello (PM) and Black Bear Ridge (BBR) based on Muttoni et al. (2004), Williford et al. (2007), Onoue et al. (2016). The BBR data from Onoue et al. (2016) has their original inferred data trend (blue line) and a more 'optimistic', speculative, interpretation of the $\delta^{13}C_{carb}$ data in black dashed line, which seems to show some of the fluctuations in $\delta^{13}C_{carb}$ as also seen at PM. The main features are the rise in $\delta^{13}C$, (1) across the T2 turnover, the plateau ((2) in figure) in positive values and the decline (3) above the T3 turnover. The carbonate isotope data from Hangwang shows a quite different response, which is likely diagenesis-impacted. The grey interval is the CNB suggested by Jin et al. (2019), is a proxy for the correlated PM4r/HQ2r magnetozones. (Hounslow)

Table. 3. Proposed choices for the Carnian-Norian boundary within the two candidate sections. This also lists the secondary markers which have varying degrees of potential for correlation, some untested.

choices	A	B	C	D
Primary marker	**FO of *Me. parvus***	**FO of *H. austriaca***	**FO of *H. austriaca***	**FO of *Me. parvus***
Section	**Pizzo Mondello**	**Black Bear Ridge**	**Pizzo Mondello**	**Black Bear Ridge**
GSSP 'spike' location.	sample NA35	Base of Bed 22	Sample FNP135A	Base of Bed 18c
Biological secondary markers	• LO *Me. praecommunisti* (ca. 0 m below NA35) • LO *Me. dylani* (ca. 2m below NA35) • LO *Gonionotites italicus* subzone, Spinosus Zone (Tuvalian 3, II) (PMAM22bis at 2.5 m below NA35) • LO *Halobia lenticularis* (FNP118, ca. 0 m below NA35) • LO *Ca. orchardi* (NA33, 6m below) • LO. *Ca. psuedodiebeli* (NA32, 7.5 m below).	• LO *Me.parvus* (bed 21f. 0.6m below) • FO *Guembelites clavatus* (bed 22b, 0.2m above)- Kerri Zone indicator • LO of diminutive *Pa. destinae* β, *Pa. johnpauli, Pa. willifordi and Pr. rhomboidale* (bed 21f, 0.6m below). • Beginning of stable populations of *Acuminatella* and *Primatella, +/- Norigondolella* species (bed 21g, 0.4m below) • See below for others	• LO *Me. echinatus* (*Pa. destinae* β), FNP138.1, ca. 2 m above FNP135A. • FO *Dimorphites noricus* (NA42.1) ca. 3.5 m above FNP135 (first subzone of Jandianus Zone) • FO *Ca?. gulloae* (*Primatella* species according to Orchard, 2019), NA43, ca. 0 m below FNP135A. • FO *Norigondolella trinacriae, Ep. spatula*, *Ep. uniformis* (PM30a, 2m above) • FO advanced epigondolellids, assigned to *E. rigoi*), (PM28a, 4m below). • FO *Ep. trangularis*, (NA43a, 7.5 m above)	• LO of *H. septentrionalis* and FO of *H. selwyni* (in bed 18d, 0.1 m above) • FO *Pterosirenites* cf. *auritus* at BBR (in bed 18d, 0.1 m above) • FO *Pr. asymmetrica*, *Pr. bifida*; *Pr. rhomboidale* (bed 18c). • LO *Me. dylani* (in 18f, ca. 0.5 m above 18c) • *FO Pa. destinae*, *Pa. irwini, Pa. permica* (bed 17c, ca. 0.6 m below 18c) • LO *Qu*. (*Me.) praecommunisti* (in 18h, ca. 0.75 m above 18c) • See below for others
Chemo-physical secondary markers	• Base of PM4r between sites PM25 and PM26, (within 1 metre of NA35) • At start of rise to more positive $\delta^{13}C_{carb}$	Ca. 1.8 m below a negative $\delta^{13}C_{carb}$ excursion peak?	Mid part of PM5n (40% into PM5n)	• At a small positive peak in $\delta^{13}C_{org}$ • Oxygen isotope (in conodonts) drop within *parvus* Subzone
Wider regional relationship	• Magnetozone PM4r allows correlation to many other sections, (especially Newark Supergroup cyclostratigraphy). • Ammonoids allow comparison to Feuerkogel F5 and Jomsom sections.	• Coincident[1] or near top of the Macrolobatus Zone (Fig. 5 in Orchard, 2019). • Near base of radiolarian assemblage 5 (FO of index *Capnodoce fragilis*) • Beginning of strata with	• Magnetozone PM5n allows correlation to many other sections, (especially Newark cyclostratigraphy). • Ammonoids allow comparison to Feuerkogel F5 and Jomsom sections.	• Within the upper part of the Macrolobatus Zone (Fig. 5 in Orchard, 2019) • Near the base of boreal Kinasovi Zone (from *Pterosirenites* cf. *auritus*) in Boreal Realm.

		Norigondolella navicula in Boreal Realm.		• Base of radiolarian assemblage 4 (esp. *Capnodoce malaca*, *Dumitricasphaera elegans*, and *Hetalum parvum*)
Estimated duration to closest secondary marker*	Ammonoid LO=120 kyr Halobia LO= 0 kyr Conodont LO= 0 kyr PM4n-PM4r boundary= ~50 kyr	Ammonoid FO =50 kyr Conodont LO= 150 kyr Conodont FO=250 kyr	Ammonoid FO= 160 kyr Conodont FO= 0 kyr Conodont LA=106 kyr Base PM5n= 200 kyr	Ammonoid FO= 25 kyr Halobia FO/LO= 25kyr Conodont LO= 125 kyr

FO= first occurrence, LO= last occurrence. In black= conodonts, in blue= Halobia, in red= ammonoids, green= radiolarians.

*Since, a GSSP point is chronostratigraphic level, a consideration of time is important. As a rough estimate of the duration using height differences, the duration of the range of *Me. parvus* at PM can be estimated using the cyclostratigraphic duration scale (*Me. parvus* range= base PM4r to mid PM5n) in the Newark Supergroup from Kent et al. (2017), which gives an estimated duration from FO to LO of *Me. parvus* of 0.75 Myr at PM. The *Me. parvus* range at BBR and PM in metres is about 3.0 m and 16 m respectively. So, for a 10 kyrs duration this gives a sediment thickness of about 4 cm and 21 cm at BBR and PM respectively. Or for 100 kyrs duration, 0.4m and 2.13 m at BBR and PM respectively. The secondary markers which are greater or equal to an estimated 0.25 myr duration from the primary marker are in grey (ca. = 1.0 m distance at BBR, ca. =5.3 m distance at PM).

[1] Macrolobatus Zone is aligned on LO of *Me*. *parvus*, based on the absence of *Anatropites* in the youngest Macrolobatus fauna listed in Fig. 5 in Orchard (2019).

Other biological secondary markers at Black Bear Ridge, Option B: •LO of *Primatella bifida* and *Pr. rotunda* (bed 23, ca. 1.0 m above).FO *Acuminatella curvata* (bed 23, ca. 1.0 m above); FO of *Ng. norica* (bed 25, ca. 3.0 m above). Most species of *Kraussodontus, Metapolygnathus, Parapetella*, and *Quadralella* disappear by end of the *parvus* Subzone.

Other biological secondary markers at Black Bear Ridge, Option D: FO *Acuminatella acuminata* and *Parapetella posterolata* (bed 17, ca. 1.5 m below 18c) ;*FO Pa. prominens* and *Primatella triangulare* (bed 17a, ca. 1.3 m below 18c). FO of *Pr. circulare*, and the diminutive *Pa*. n. sp. D of Orchard (2014), *Pa. johnpauli, Pa. pumilio,* and *Pa. willifordi* (beds 18e-f, ca. 0.5 m above 18c).

- At Pizzo Mondello, the base of magnetozone PM4r is between sites PM25 and PM26 (Muttoni et al., 2004), and the FO of *Me. parvus* is in sample NA35 (Fig. 8), so these two events are very close, making the base of magnetozone PM4r a closely coincident secondary marker for the base of the Norian.
- Several carbon isotope fluctuations occur in the interval between conodont turnovers T1 and T3, with the most pronounced positive change (indicated as (1) in Fig. 9) near the base of turnover T2, a trend to more positive $\delta^{13}C$ seen in both candidate sections in both carbonate ($\delta^{13}C_{carb}$) and organic matter ($\delta^{13}C_{org}$) (Muttoni et al., 2004, 2014; Mazza et al., 2010; Onoue et al., 2016; WIlliford et al., 2007). This provides a suitable 3rd type of secondary marker for the base of the Norian. The details of any finer resolution, global stratigraphic changes in $\delta^{13}C$, within the T2 to T3 interval, are currently unresolved (see section 4.3).

(Nicora, Orchard, Rigo, Hounslow)

3. KEY ATTRIBUTES OF THE FIRST OCCURRENCE OF *HALOBIA AUSTRIACA* AS A PRIMARY MARKER TO DEFINE THE BASE OF THE NORIAN

Several workers have suggested that the FAD of the bivalve *Halobia austriaca* could act as a good proxy for correlation of the Carnian- Norian boundary (Krystyn & Gallet, 2002; Levera & McRoberts, 2008; McRoberts & Krystyn, 2011; Levera, 2012). Here, the merits of using *H. austriaca* as a primary marker for the base of the Norian are explored, and its potential for high resolution correlation. This section should be read in conjunction with McRoberts (in press) a draft of which was seen by the CNB working group prior to publication, which has more details of the taxonomic issues and particularly discusses North American occurrences of *Halobia austriaca.*

Overview: *Halobiids* are an extinct family of thin-shelled bivalves, which proliferated during the Late Triassic, which was an interval of rapid evolutionary change in *Halobia*, with a turnover rate that matched or exceeded that of ammonoids (McRoberts, 2010, 2011). Thin-shelled bivalves have also been used elsewhere in the Phanerozoic to define stage bases. The FAD of the inoceramid bivalve *Platyceramus undulatoplicatus* has been used to define the base of the Santonian (Lamolda et al., 2014); and probably an inoceramid bivalve may be used for the forthcoming GSSP of the Coniacian (https://stratigraphy.org/gssps/). A 1970s definition of the base of the Telychian Stage (Early Silurian) also used a brachiopod primary marker (https://stratigraphy.org/gssps/).

In these respects, use of *H. austriaca* to define the base of the Norian would be consistent with usage at some other GSSP's. The fact that it is a macrofossil also has additional merit, in that specialists could identify it in the field. *Halobia austriaca* is also a long-standing species (Mojsisovics, 1874), and has a distinctive form (Figs. 10, 11) because of its outline and pattern of ribbing (Levera, 2012; McRoberts, in press). Synonyms of *H. austriaca* are also quite well understood (Levera, 2012; McRoberts, in press).

In parallel with the conodont work at Black Bear Ridge and Pizzo Mondello, McRoberts (2011) and Levera (2012) have produced major taxonomic studies of *Halobia* from the candidate sections. Also, Krystyn (1980) and Krystyn & Gallet (2002) summarised

the distribution of *Halobia* near the CNB in Austria and the eastern Mediterranean, with some updates of these data in McRoberts (in press).

3.1 Evolutionary trends, origin and taxonomy of *H. austriaca*

Halobia are thought to be several separate lineages derived from ancestors of *Daonella*. This evolutionary transition may be near the base of the Carnian, either directly or through the genus *Aparimella* (McRoberts, 2010). At the moment the species level phylogenetic lineage of *H. austriaca* is uncertain, with a number of possible pathways (McRoberts, in press).

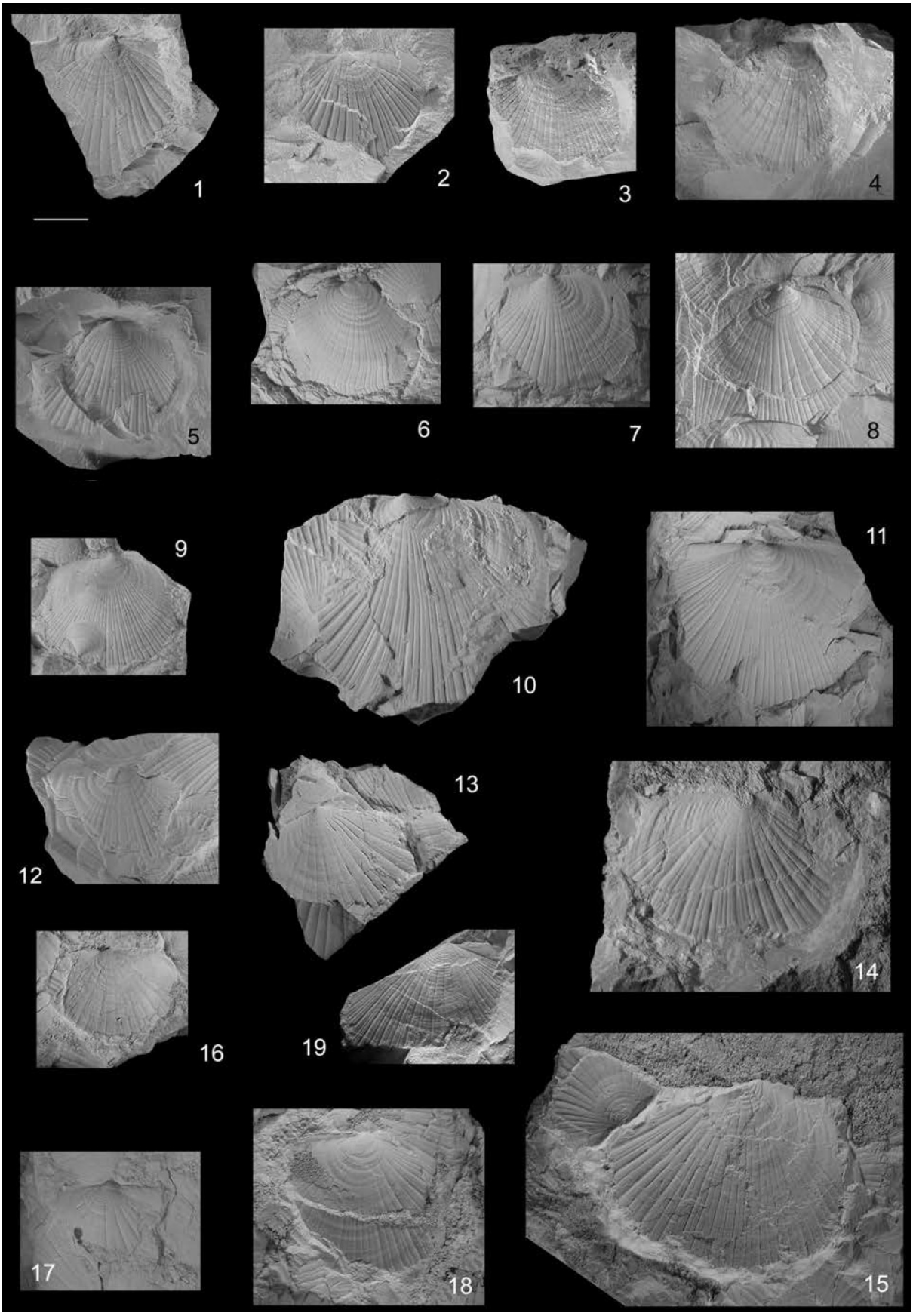

Fig. 10. Specimens of *H. austriaca* from Pizzo Mondello (from Levera, 2012).

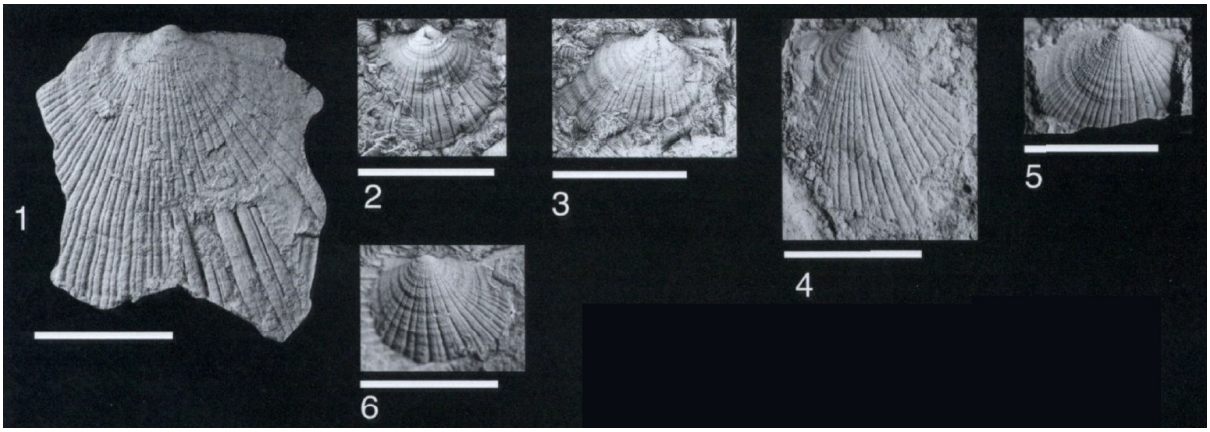

Fig. 11 Specimens of *H. austriaca* from Black Bear Ridge (from McRoberts, 2011). More specimens are illustrated in McRoberts (in press).

At the species level, the variety and variability in *Halobia* probably requires further critical taxonomic work to consolidate these. Over the last 100 years, work has led to the proliferation of species, many of which are based on inadequate material (small sample sizes, taphonomically compromised, without regard to population morphological variability; McRoberts, 2010, in press). Of the 300 or so species of *Halobia* assigned, McRoberts (2010) suggested around 30 may be valid. The re-evaluation of *H. austriaca* by McRoberts (in press) is part of this process.

Morphologic evidence suggests *Halobia* may have either had an epibyssate life mode (weakly attached to floating algal debris?), or a freely resting/reclining mode without byssal attachment. The lack of clearly demonstrated attachment tends to support the later. The thin shells and low profiles suggest a streamlining response. *Halobia* have a strong association with oxygen deficient water masses and sediment, without major evidence of post-mortem transport. Seilacher (1990) proposed that *Halobia* housed symbiotic sulphur-utilising bacteria, which is why they had a preference for oxygen poor environments. The episodic nature of often monospecific *Halobia* shell beds suggests a low resistance to disturbance and ability for rapid recovery.

Wider occurrence: *Halobia austriaca* is fairly widely spread throughout the southern and northern hemispheres (New Zealand to Alaska) and in low to high palaeolatitudes (eastern Tethys, e.g., Turkey to near the N. paleopole in NE Asia and Siberia) (Table 3, and data in McRoberts, in press). It occurs in the truly oceanic carbonate and chert realms in Japan, Timor and Oman (Shackleton et al., 1990) to deep water turbiditic systems in the western Quinling in China (Meng et al., 2007). Both carbonate and clastic deeper and open water systems accommodated *Halobia*. Shallow water settings seemed to be less accommodating to *Halobia* (Del Piero et al., 2020). This wide distribution of *H. austriaca* (and other halobiids in general) is thought to be due to halobiid opportunism, and probably having a larval planktonic early life stage, allowing colonisation of widely spread suitable habitats.

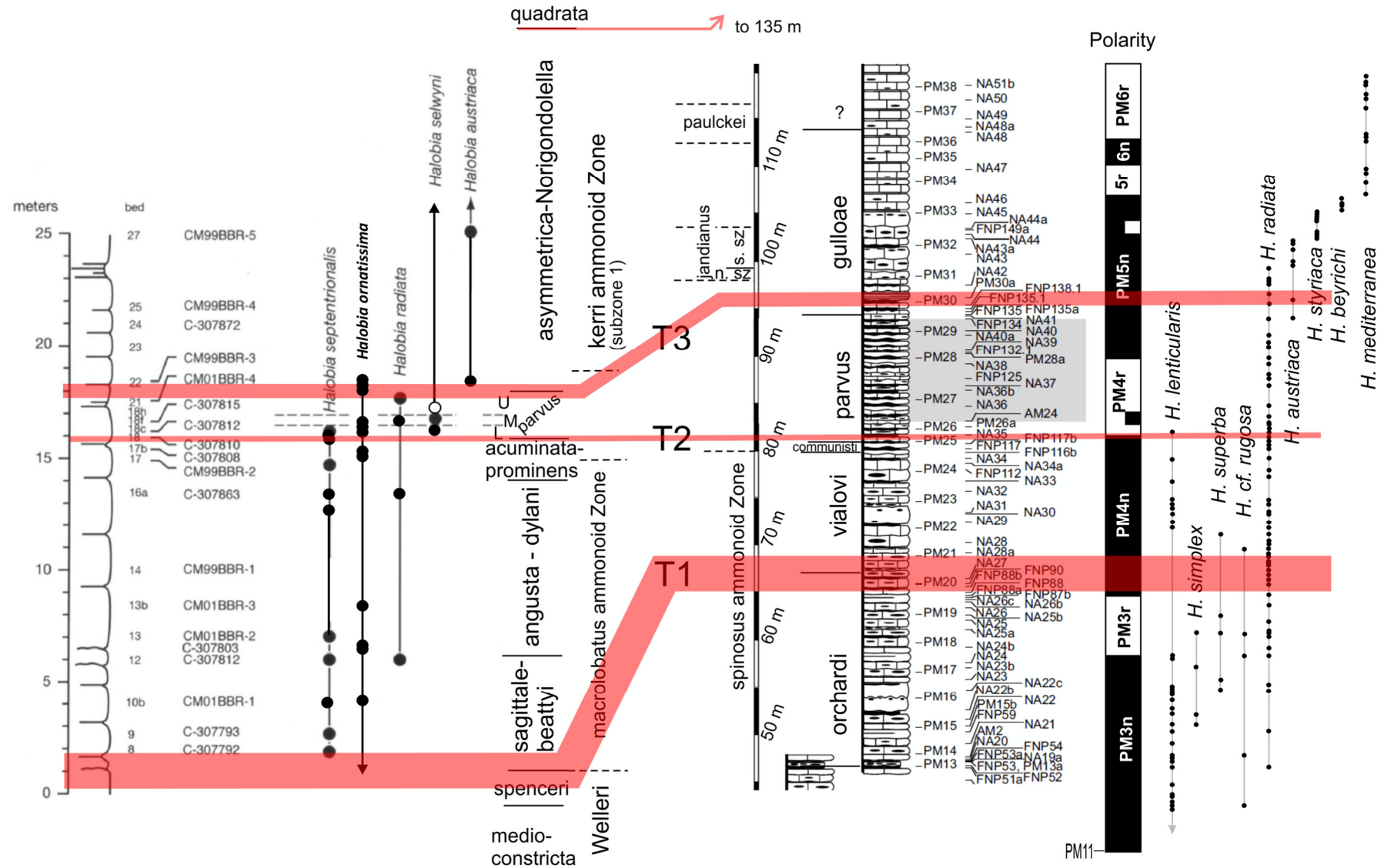

Fig. 12. *Halobia* occurrences at Black Bear Ridge (McRoberts, 2011, in press) and Pizzo Mondello (Levera, 2012; Balini et al., 2012), with the conodont turnovers, T1, T2, T3 (Mazza et al., 2018; Orchard, 2019) used for correlation between these two sections. Magnetostratigraphy from Muttoni et al. (2004) with boundaries placed according to the PM sample positions in the log from Mazza et al. (2012a).

This global distribution is a great strength of using *H. austriaca* for correlation and GSSP definition. However, like many macro fossils, episodic occurrence (perhaps less severe than in Late Triassic ammonoids) in sections can limit cm to meter scale resolution studies, which is probably part of the reason there are very few section-focused studies and rather more formation- and site-focused studies (Table 4).

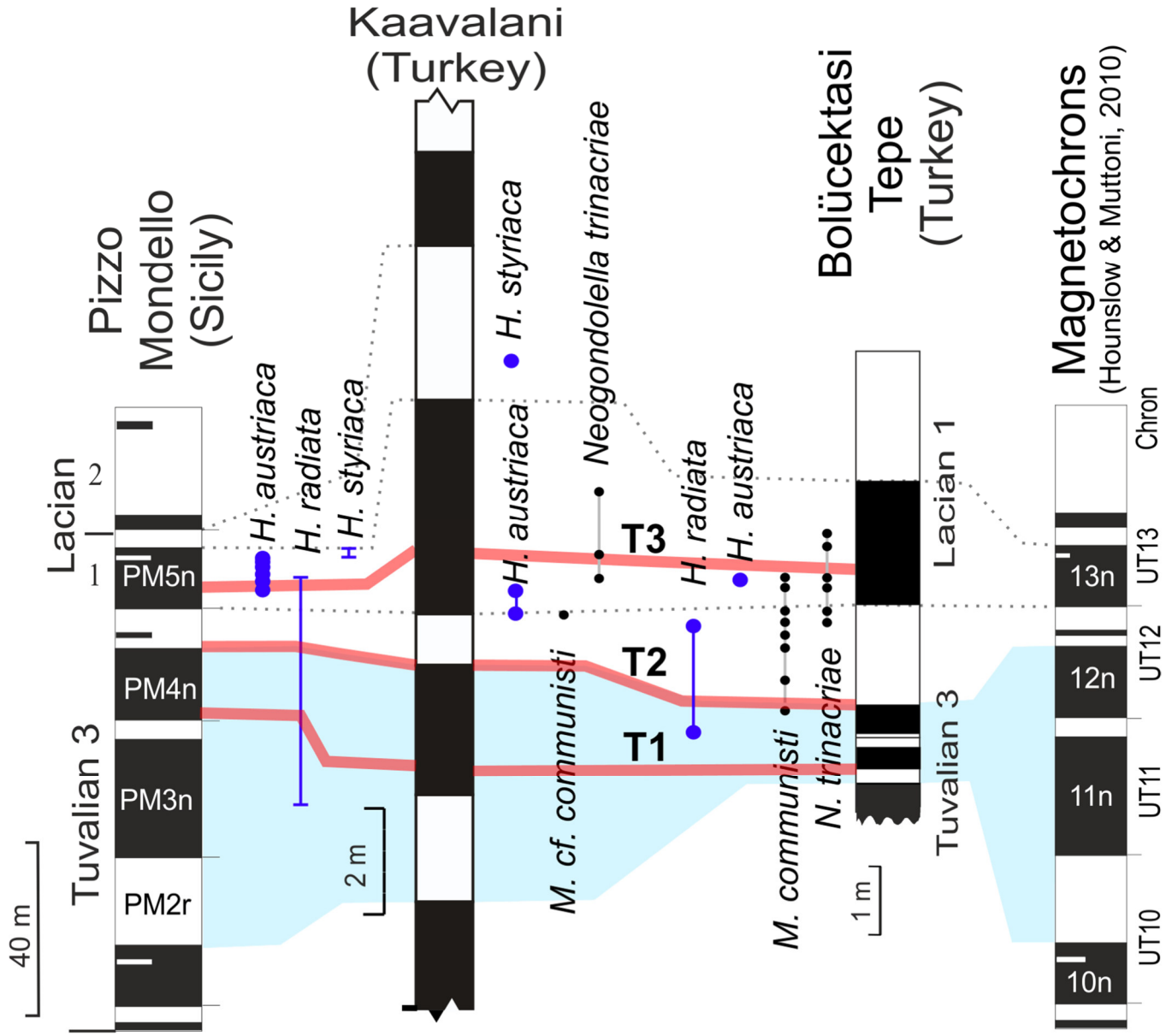

Fig. 13. Relationships between *Halobia* occurrences, selected conodonts and magnetostratigraphy in the Pizzo Mondello, Kaavalani, and Bolücektasi Tepe sections (based on data in Gallet et al., 2000; Krystyn and Gallet, 2002, updated by Krystyn). Blue and dotted lines are magnetostratigraphic correlations, red the correlated conodont turnovers (correlated using position in magnetozones at Pizzo Mondello). Data for Turkish sections updated by Krystyn.

3.2 Halobia austriaca: reliability and correlation with physical and biotic events

The relationship between *H. austriaca*, conodonts and ammonoids (and geomagnetic and geochemical data) is best defined in section-based data. This can readily be seen Table 4, where *H. austriaca* is apparently associated with a variety of ammonoids and conodonts, which have a typical late Carnian (Tuvalian) (e.g., *Sirenites senticosus*) to early Norian (Lacian) (e.g. *Juvavites* sp.) age range.

This apparent wide range in age of *H. austriaca* (in non-section-based datasets), is probably due to lumping together occurrences over a wide stratigraphic range. The most complete and comprehensively integrated datasets around the CNB, with large collections of *Halobia,* are those from Black Bear Ridge and Pizzo Mondello (Fig. 12). Krystyn & Gallet (2002) also describe *H. austriaca* occurrences associated with conodont, ammonoid and geomagnetic data from sections at Silikcá Brezová, Kaavalani, Bolücektasi Tepe and Feuerkogel (Fig. 13; McRoberts, inpress). The exception to this two-fold division in data-quality, are the ranges of *Halobia* species in western North America described by McRoberts (2010, 2011, in press), from a range of stratigraphically better constrained occurrences, allowing a 'calibration' against North America ammonoid zones (Fig. 14). However, Balini et al. (2012) have argued "…. it is conceptually wrong to use data from scattered localities, ….. to calibrate cm-by-cm sampled sections".

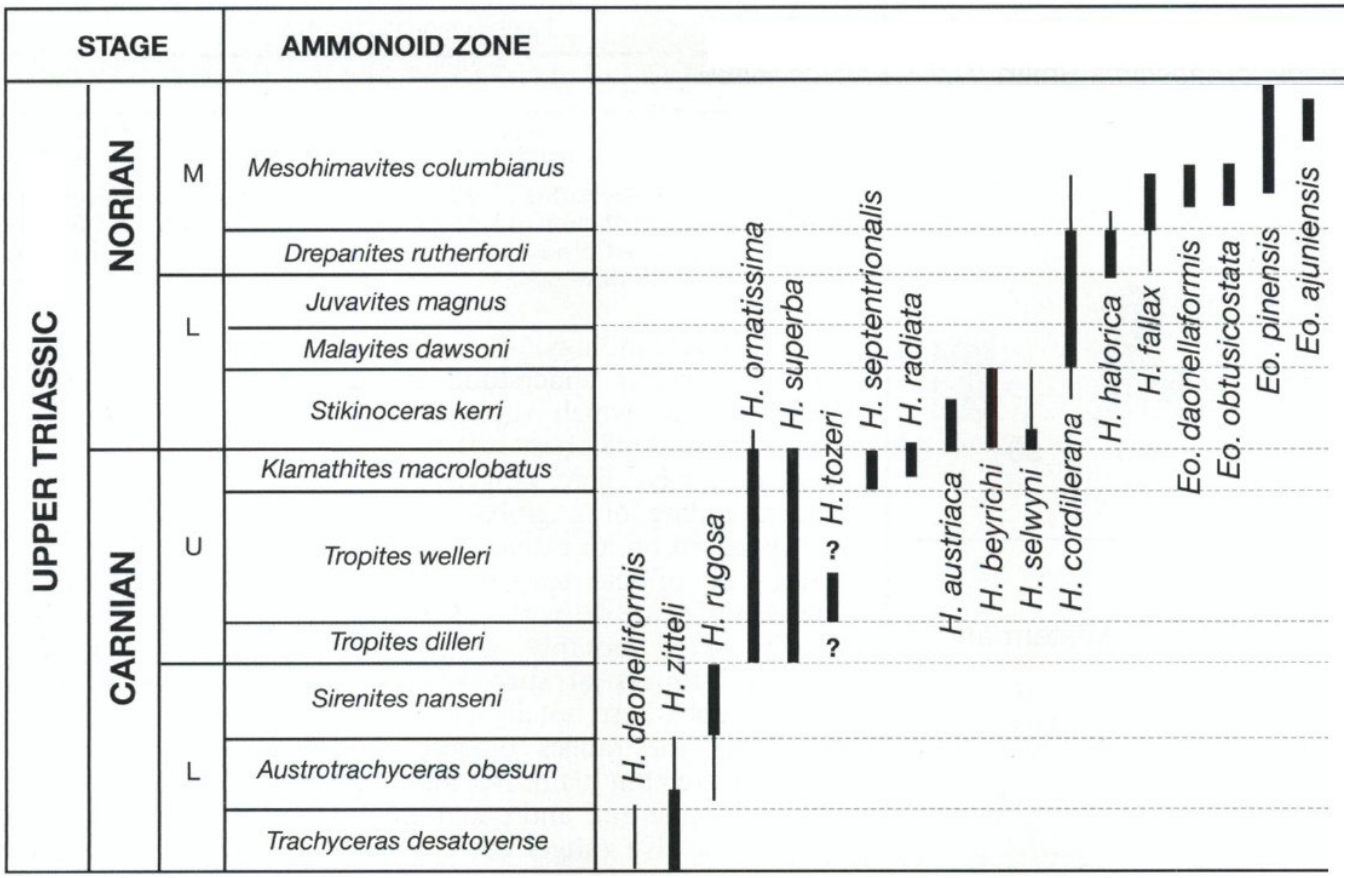

Fig. 14. Ranges of *Halobia* against northern American ammonoid zones (from McRoberts, 2011).

The section-based data from Black Bear Ridge and Pizzo Mondello show the FO of *H. austriaca* at around the T3 conodont turnover near the last occurrence of *Me. parvus* (top of Parvus Zone/Subzone; Fig.12). The re-assessment of the North American faunas over the last 10 years by McRoberts (in press) is substantially different from previous evaluations (McRoberts, 2011), with the lowest assured occurrence in bed 22 at Black Bear Ridge (Fig. 12). Across Williston Lake at Pardonet Hill East (Table 3), possible juveniles of ?*H. austriaca* (or more probably *H. selwyni*) occur in the lower part of the Parvus Zone (C-307835. bed 3 and C-307836, bed 4 at Pardonet Hill; McRoberts, in press). These two levels also contain *Gonionotites*? sp. and *Pterosirenites auritus*. Further details of *H. austriaca* in North America are in McRoberts (in press). Notably, at both Black Bear Ridge and Pizzo Mondello the last occurrence (LO) of *H. radiata* is also near to the T3 conodont turnover (or upper part of Parvus Zone), suggesting that the LO of H. *radiata*-FO H. *austriaca* transition may be a useful approximate

proxy for this level, and not far above the base of the *Stikinoceras kerri* ammonoid Zone and *Guembelites jandianus* Zone (Figs. 12, 14; Balini et al., 2012).

In Austrian and Turkish sections (Fig. 13) Krystyn & Gallet (2002) associated the occurrence of *H. austriaca* broadly with the range of '*Me. communisti* morphotype B' (a form species now in part re-assigned to various *Primatella species* by Orchard (2013), *Me. communisti multinodosus* by Noyan & Kozur (2007); Mazza & Martinez-Perez (2015), and in the Turkish sections synonymous with *Neogondolella trinacriae* (McRoberts, in press). At Pizzo Mondello *Me. communisti* has a restricted range from within magnetozone PM4n to PM5n (UT12n to UT13n magnetochrons; Fig. 8), largely between the T2 and T3 conodont turnovers (Mazza et al., 2012a), much like that in the Turkish sections (Fig. 13). As at Pizzo Modello, *H. austriaca* is found in the magnetochron UT13n at Bolücektasi Tepe, but lower at Kaavalani within the topmost part of magnetochron UT12r (Figs. 12,13). Therefore, possibly as at Pardonet Hill in British Columbia, the FO of *H. austriaca* in the Kaavalani section is a little lower (around the mid Parvus Zone) within the T2 to T3 interval (compare Figs. 12,13). Consequently, the most detailed data from Pizzo Mondello suggest a polarity zone boundary is not closely coincident with the FO of *H. austriaca,* and hence- perhaps the lower part of magnetochron UT13n is missing in the Kavaalani section*?*

Secondary Markers: If *H. austriaca* were chosen as the primary marker for the base of the Norian, then the upper boundary of the Parvus Zone (subzone) and conodont turnover T3, or 'traditional Norian' ammonoids may be suitable secondary markers (Table 3). That is, the base of the *Stikinoceras kerri* Zone (with *Guembelites*) in North America and base of the *G. jandianus* Zone in the western Tethys. In NE Asian sections if the synonymised *Indigirohalobia* (*Popowihalobia*) *brooksi* and *Indigirohalobia* (*Primahalobia*) *kilganaensis* represent forms of *H. austriaca*, then the association in NE Asia (Table 3) is with the ammonoid *Sirenites yakutensis* and the Halobiid Zone *Indigirohalobia asperella* (especially upper part). The details of this relationship to NE Asians sections would need clarification.

(Hounslow, Krystyn)

Location	**Fauna associated with *Halobia austriaca* occurrences (and its synonyms)**	**Section details**	**Reference**
McCarthy C-5 quadrangle, Alaska	*Discophyllites* cf. *D. ebneri* ; *Juvavites* sp. Indet {T/L}	no	MacKevett, 1971, Silberling, 1963
S.W. coast of of Bostwick Inlet, Gravina Island, Alaska	*Arcestes* sp. , *Juvavites (Anatomites) externiplicatus* {T} (all in float)	no	Berg & Cruz, 1982
Herring Bay, Admiralty Is., Alaska	*H. ornatissima, H. lineata, Margarites cf. jokelyi, Juvavites externiplicatus, J. knowltoni, J. cf. subinterrutptus , Arcestcs shastensis, Pinacoceras cf. rex, Aulacoceras cf.carlottense* {T}	no	Smith, 1927
Pardonet and Baldonell fms , East Pardonet Hill, Brown Hill, British Columbia, Canada	*Stikinoceras kerri* Zone	yes	McRoberts, 2011
Alaska Canyon, Jackson Mt, Humboldt County, Nevada	*Halobia superb,* (overlying are *Arcestes pacificus*; *Discotropites ojsvarensis* {T}	yes	Fuller, 1986
Wallowa terrane, Oregon, USA	*Halobia cf. lineata*	no	Stanley et al., 2008; McRoberts, 1990
Section F1-E, Feuerkogel, Austria	*Metapolygnathus communisti* morphotype A, *Neogondolella trinacriae, Epigondolella abneptis, Primatella primitia, E. abneptis, Norigondella navicula.*	yes	Krystyn, 1980; Krystyn & Gallet, 2002
Section B, Feuerkogel, Austria	*M. communisti* morphotype A and *Neogondolella trinacriae, E. abneptis, Pr. primitia, N. navicula.*	yes	Krystyn, 1980; Krystyn & Gallet, 2002
F 4 and F 5 N. Feuerkugel, Austria	*M. communisti; E. abneptis,. Pr. primitia, N. navicula; Dimorphites noricus. Griesbachites* sp.,	yes	Krystyn, 1980; Krystyn & Gallet, 2002
Silicka Brezova, Slovakia	*M. communisti* morphotype A and *Neogondolella trinacriae, Carnepigondolella pseudodiebeli, N. navicula.*	Yes	Krystyn & Gallet, 2002
Izvorul Malului klippe, Romania	*H. styriaca*, *H. falax*, *H. bukovinensis*, *Monotis* cf. *haueri*	no	Popescu & Popescu, 2008
Dachstein Limestone, Vaşcău plateau, Romanian	*H. austriaca, H. superba*, *H. styriaca, Gondolella (Quadralella) polygnathiformis, E. abneptis, Enantiognathus ziegleri, and Prioniodella ctenoides*. Overlying strata have *H. styriaca, H.* cf. *beyrichi, Monotis* ex gr. *haueri* ; *Juvavites (Anatomites) ducetii* {L}	no	Bucur, 2001
Kaavalani, Turkey	*M. communisti* morphotype A; *C. pseudodiebeli, Placites placodes* {L}	yes	Krystyn & Gallet, 2002; Gallet et al., 2000.
Bolucektasi Tepe, Turkey	*M. communisti* morphotype A and *Neogondolella trinacriae, C. pseudodiebeli,*	yes	Krystyn & Gallet, 2002; Gallet et al., 1992
Turkestan flyscoid belt, Afghanistan	*Sirenites senticosus*, {J} *Monotis* sp.	no	Montenat, 2009
Sabau river NE of Kapan in West Timor	*Halobia clari*	no	Kristan-Tollmann et al. 1987; Charlton et al., 2009
Kanikeh Formation, Kalimati, Wai Lola Kecil River, Seram Is., Indonesia	*H. styriaca, H. austriaca*, *Monotis hoernesi*, *H. superba*	no	Wahyudiono et al., 2018
Oreti River, New Zealand		No?	Raine et al., 2012, Campbell, 1994
New Siberian islands, exposure 190,	(9–13 m) ammonoids *Arctophyllites* cf. *popovi; Zittelihalobia fallax*	yes	Konstantinov et al., 2003

Tikhaya River	(17–18 m) bivalves *Halobia* ex gr. *austriaca, Z. indigirensis, Z. fallax; Z.*aff. *obruevi*		
Anyui–Chukotka Fold System, Northeastern Asia	*H. superba*	no	Katkov et al., 2010
Magadan-Kolmya- Omolon, Northeastern Asia	*Sirenites yakutensis* [with *In. kilganaensis*, *H. brooksi*]	yes	Polubotko, 2005
Sirkunovskaya suite, Yana & Indigirka rivers. NE Russia	*Arctophyllites taimyrensis, Ar. popowi, Yanosirenites seimkanensis, Neosirenites armiger,* {T} *N. irregularis, Yakutosirenites pentastichus, Sirenites yakutensis, Striatosirenites kedonensis, St. kinasovi, Proarcestes gaytani, Pr. verchojanicus, Indigirohalobia popowi, In. kudleyi, H. superba, In. asperella, H.* ex gr. *brooksi, Zittelihalobia kiparisovae, In. kilganaensis, H. kegaliensis, H.kinasovi.*	no	Truschelev & Grinenko, 2016
Xinduqiao Formation, Songpan Terrane, China	*H. gigantea, H. pluriradiata, H. rugosa*	no	Meng et al., 2007
Qugasi Formation, Qinghai-Xizang Plateau, China	*Discophyllites ebneri, Joannites sp., Proarcestes sp., Lobites* sp. and *Sturia sp.*, {D/J}, *H. yunnanensis, H. convexa*.	no	Lin et al., 2007
Bayanhar Group, NW Leixiwudanco and NE Malanshan, Qinghai-Xizang Plateau, Hohxil, China	*H. yunnanensis, H. convexa ,H. banmaensis,H. cf. yandongensis*	no	Sha & Grant Mackie, 1996
Pane Chaung Group in Bhopi Vum Area, Myanmar	*H. dalliana, H. styriaca, H. dilatata, H. tozeri, H. comata, H. mediterranea*, *Daonella* sp., ?*Judicarites* sp. and *Posidonia* sp.	no	Tun Min & Maung, 2019
Nam Mu Formation, N. Vietnam	H. talauana,H. substyriaca, H. superba, *Margaritropites fongthoensis,*{T} *Juvavites* sp. and *Discotropites* sp. {T}	no	Komatsu et al., 2017; Khuc, 1991
N. Thailand	*Margaritropites phongthoensis* {T}*, H. talauana, H. styriaca, H. substyriaca, H. austriaca, Z. posterolaevis, Z. rugosa, Indigirohalobia pluriradiata*.	no	Khuc & Huyen, 1998

Table 4. List of occurrences of *Halobia austriaca* (and its probable synonyms), and associated fauna (listed at same sampling locality or section). Ammonoids in red, conodonts in blue (most not revised from original description). This does not include the two candidate sections at Pizzo Mondello and Black Bear Ridge. Kristan-Tollmann et al. (1987) also has a map of the distribution of *H. austriaca* globally, and McRoberts (in press) also discusses more locations. Details on more locations of *H. austriaca* in Greece, Hungary, the Himalayas, Bosnia, Japan and California are discussed in Levera (2012).

Some *H. superb, H. gigantea* have many similarities to *H. Ornatissima* for which the latter is a junior synonym (McRoberts, 1990; 2011).

Halobia (Zittelhalobia) rugosa is similar to *Halobia septentrionalis* (McRoberts, 2011).

Halobia beyrichi and H. mediterranea are similar to the North American H. selwyni (McRoberts, 2011)

Indigirohalobia kilganaensis is a probable synonym of *Halobia austriaca* (McRoberts, inpress)

Ammonoid assemblage ages: {D}= Ladinian ammonoid, {J}= Julian, {T}=Tuvalian, {L}=Lacian (by Krystyn).

4. OTHER CORRELATION ISSUES

4.1 Correlation potential into high palaeolatitudes

The species *Halobia austriaca* Mojsisovics, 1874 has been described many times and reviewed in atlases on Triassic faunas for Northeast Asia (Kiparisova, 1947; Vozin & Tikhomirova, 1964; Bychkov et al., 1976). According to Bychkov et al. (1976) and Dagys et al. (1979), this species appears in Northeast Asia in the *Sirenites yakutensis* Zone, there considered Upper Carnian. Subsequently, the *S. yakutensis* Zone was subdivided (Konstantinov & Sobolev, 2000a; 2000b; Konstantinov, 2019) into (from bottom to top) the *Sirenites* (= *Orientosirenites*) *yakutensis* Zone proper, *Orientosirenites bytschkovi* Zone, *Striatosirenites* (= *Kedonosirenites*) *kedonensis* Zone and *Striatosirenites* (= *Omolonosirenites*) *kinasovi* Zone. The *yakutensis*, *bytschkovi*, and *kedonensis* zones, together with the underlying *Yakutosirenites pentastichus* Zone, are now considered by Russian workers to largely relate to the Upper Carnian. In the absence of a GSSP, the lower boundary of the Norian in Northeast Asia has, since 2002, been widely considered as the base of the *kinasovi* Zone by Russian workers. The *Omolonosirenites kinasovi* Zone is reliably correlated with the lower subzone of the *Stikinoceras kerri* Zone in British Columbia, since common in both these zones are the species *Pterosirenites auritus* Tozer and *Pinococeras regiforme* Diener. In addition, *P. verchojanicum* Archipov (zonal index of *Pinacoceras verchojanicum* Zone overlying the *kinasovi* Zone) has a smooth shell and a less complex suture, and most likely belongs to *Pinacoceras* sp. indet., described by E.T. Tozer in the lower subzone of the *Stikinoceras kerri* Zone (Tozer, 1994; p. 131, table 110, fig. 4).

The zonal scale of halobiids in the Upper Triassic of northeastern Russia (Polubotko, 1986, 2005) places the lower boundary of the *kinasovi* Zone within the *Zittelihalobia (Obruchevihalobia) kiparisovae* beds. However, *H. austriaca* was not assigned by Polubotko to the suite of halobiids from both of these beds, nor in the complexes of the *Indigirohalobia (Popowihalobia) asperella* Zone and I. (P.) *indigirensis* Zone. In the opinion of I.V. Polubotko (pers. comm to Konstantinov, 2020), *Halobia austriaca sensu stricto* is certainly present in Northeast Asian sections, but it is currently impossible to accurately determine the level of the first appearance of this species in these sections and compare it with the modern ammonoid zonal scale. To use *H. austriaca* in NE Asia sections it would be necessary to revise the most representative sections and taxonomic composition of halobiids in the CNB interval. Despite these circumstances, it is clear that the species *Halobia austriaca* Mojsisovics has a very high potential for correlation due to its almost cosmopolitan distribution at all paleolatitudes (Table 4).

In the Svalbard Archipelago (i.e., Hopen Island) the Flatsalen Formation contains the ammonoids '*Pterosirenites'* (= *Norosirenites*) *nelgehensis* (Archipov) and 'P.' (=N.) *obrucevi* forma *nabeshi* McLearn (Korchinskaya, 1982), which are correlated with beds in NE Asia containing *Norosirenites nelgehensis* and beds with *Norosirenites obrucevi* – i.e., equivalent to most of the *Pinacoceras verchojanicum* Zone (Konstantinov & Sobolev, 2000b). Since the latter overlies the *kinasovi* Zone in the sections of Northeast Asia, the basal Norian (i.e., base the *kinasovi* Zone proxy) must be in the underlying unit (the upper part of the De Geerdalen Formation or lower part of the Flatsalen Formation), which are without ammonoids.

Currently, there are problems in tracing stage boundaries in the Boreal Triassic using conodonts (Konstantinov & Klets, 2009). For example, in NE Asia, conodonts are practically unknown in the Induan stage; and are rarely found in the terrigenous rocks of the Middle and Upper Triassic, where they are limited in distribution to a few individual levels.

(Konstantinov)

At present little is known about biostratigraphic events in the pollen/ spore or in the marine algae (dinoflagellate cysts) records that would correlate closely with the proposed CNB markers. However, in the Barents Sea and Svalbard, the palynofloral succession across the boundary interval inferred by the ammonoids (i.e. the approximate De Geerdalen- Flatsalen boundary) is remarkably consistent and easily recognisable in this area (Paterson & Mangerud, 2020.). This includes the first regional occurrence of several distinctive taxa, including *Cingulizonates rhaeticus, Kyrtomisporis gracilis, K. laevigatus, Limbosporites lundbladiae* and *Retitriletes austroclavatidites*. However, due to provincialism, these occurrences significantly predate the first occurrences of the same taxa in central and southern Europe, so they are unlikely to aid correlation with PM, but could permit correlation to British Columbia, if palynological data could be gathered. Also described from the Flatsalen Formation (on Hopen) in the 1970-1980's are *Halobia aotii*, *H. fallax*, *H*. cf. *maximiliani* and *H*. cf.*ovbruchi*, but they have no modern re-study or proper evaluation. A search for conodonts in the upper De Geerdalen and Flatsalen formations (by Orchard & Hounslow) failed to yield any useful specimens.

(Paterson, Kürschner, Hounslow)

4.2 Radiolarians at the Carnian-Norian Boundary

Radiolarian faunas from the Upper Carnian and Lower Norian are known from several regions of the world, e.g., USA, Baja California Mexico, Western Europe, the Mediterranean, Japan, the Philippines, Timor and the Arctic. However, the best documented successions across the CNB thus far are those from Haida Gwaii (British Columbia) where seven radiolarian assemblages are intercalibrated with the conodont zones established at Black Bear Ridge (Carter et al., 1989, Carter & Orchard, 2000; 2011; 2013).

The radiolarian succession is characterized not by any notable extinction events but rather by the progressive appearance of new species (and over 20 new genera) ranging upward through the boundary interval. Over 35 of these species range from their lowest occurrence in strata age equivalent to the ('late Carnian') Welleri Ammonoid Zone, through the ('early Norian') Kerri Ammonoid Zone.

Based on the study of over 140 species from 44 faunules from 11 localities in Haida Gwaii, seven radiolarian assemblages (Ass.) were established and calibrated with conodont zones established at Black Bear Ridge, prior to their formal naming (Carter & Orchard, 2013). Orchard (2014, fig. 4) showed the equivalence of the conodont zone names used here. The pertinent ones for the discussion of the boundary interval are **Radiolarian Ass. 3** occurring in the Lower Primitia conodont zone (=*Ac. angusta–Me. dylani and Ac. acuminata-Pa. prominens* subzones); **Ass. 4** in the *Me. parvus* Subzone; and **Ass. 5** characteristic of the Upper Primitia Zone (=*Pr. asymmetrica – Norigondolella* Subzone).

Regarding the two possible datums for the CNB, the *Me*. *parvus* FAD corresponds to the base of Ass. 4, which is characterized by 16 new taxa, notably *Capnodoce malaca* Blome, *Capnuchosphaera crassa* Yeh, *Dumitricasphaera elegans* Tekin, *Hetalum parvum* (Tekin) and *Sepsagon asymmetricus* (Bragin). These are also known from Oregon (Blome 1983, 1984), the Philippines (Yeh 1990) and the Mediterranean regions, where they were formerly regarded as indicating the early Norian. It is notable that nearly all species first appearing in Ass. 4 are rare, becoming more common in Ass. 5 and above.

The *Halobia austriaca* FO approximates the top of the *Me. parvus* Subzone (base of the *asymmetrica-Norigondolella* Subzone) and is characterized by the appearance of 14 new taxa in **Ass. 5**, with more abundant occurrence of these appearing earlier in the *Me. parvus* Subzon*e*. Most notable of these is *Capnodoce fragilis* Blome (=*Capnodoce sarisa* De Wever), which is singularly abundant and has been widely recognized in lower Norian samples in North America (Blome 1983, 1984), the Mediterranean (De Wever et al. 1979; Tekin & Yurtsever, 2003 etc.), Japan (Yao et al. 1982, Sugiyama, 1998 and many others), and the Philippines (Yeh and Cheng 1996). This is identified as the key index taxon for recognition of the early Norian (i.e. the Kerri Ammonoid Zone). Also making their first

appearance at this level are *Syringocapsa batodes* De Wever, known from European, Mediterranean, and Far East areas (as above); the genus *Fontinella* Carter described previously from the Rhaetian (Carter 1993); and *Corum regium*, *Icrioma praecipua* and *Sarla externa,* all described by Blome (1983, 1984) from central Oregon, USA.

In summary, Ass. 4 fauna is viewed as a prelude to the more definitive changes seen in Ass. 5, which is the most distinctive radiolarian fauna marking the boundary interval. As such, these changes support using the *H. austriacum* FAD for the base of the Norian, and therefore if this were so decided the **Ass. 4/5** boundary could be a suitable secondary marker for the base of the Norian using radiolarians. These statements correct some minor textual errors in assignment of samples in Carter & Orchard (2013).

Radiolarians reported from Pizzo Mondello (Nicora et al., 2007, Balini et al., 2008, 2010) come from Upper Carnian strata and contain none of the key species that are known in Haida Gwaii, to first appear in Ass. 4 or Ass. 5 (the 4/5 boundary is at the top of the Me. *parvus* Subzone in British Columbia).

(Carter)

4.3 Isotopic changes for global correlation in the boundary interval?

4.3.1. The carbon isotopes

Muttoni et al. (2014) and Mazza et al. (2010, 2018) have shown a positive peak in $\delta^{13}C_{carb}$ at PM, of ca. 0.7 permil (Figs. 9, 15). This peak is situated around the FAD of *Me. parvus*, at the T2 turnover at the top of normal magnetozone PM4n. Is this peak also present in other sections?

Concerning BBR: The conclusion of Lei et al. (2021) that $\delta^{13}C_{carb}$ values at BBR do not represent diagenetically altered values (Fig. 15) is debatable. Values of -5 to -3 permil in $\delta^{13}C_{carb}$ are unlikely to reflect global oceanic values and may be indicative of significant diagenetic influence. With so many clay-rich samples and with a high TOC, at a conodont alteration index of ca. CAI 3, clay recrystallization could have generated reaction products (which gives values around -5 permil in $\delta^{13}C$, Kaufman & Knoll, 1995), or organic matter remineralization which moves $\delta^{13}C$ of pore fluids toward more negative values, but without necessarily changing the oxygen isotope values (e.g. Marshall, 1992).

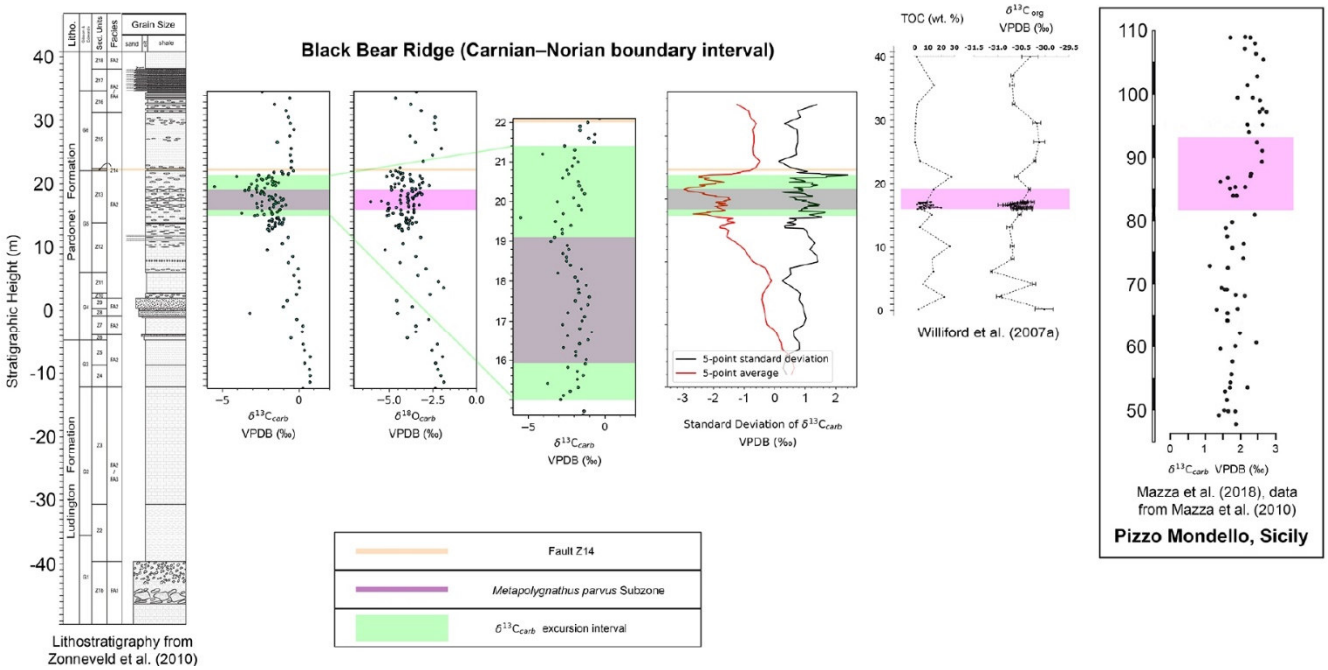

Fig. 15. The carbon isotope data from Black Bear Ridge (from fig. 2 of Lei et al. 2021). All studies are displayed with the same scale for stratigraphic height except for the zoomed (4th column) in $\delta^{13}C_{carb}$ at BBR.

Lei et al. (2021) affirm in their conclusion: "*This excursion interval displays high point-to-point variability, rapidly oscillating between anomalously low $\delta^{13}C_{carb}$ values and values comparable to the average outside of the excursion. This atypical feature is interpreted as the result of local carbon cycling being disrupted in response to the climatic perturbations at the CNB*." An alternative interpretation would be that this high point-to-point variation (green interval in 5th column in Fig. 15) is due to bed-by-bed changes in the diagenetic pathways of $\delta^{13}C_{carb}$. However, the $\delta^{13}C_{carb}$ signal does not appear to show a direct facies dependence, and the anomalously negative values are largely not observed beyond the CNB interval. Therefore, more work is needed to understand if this CNB excursion interval at BBR as due to diagenesis or is rather a diagenetic amplification of an existing primary signal or alternatively represents local water column $\delta^{13}C$ values.

The long-lasting trend observed at BBR may be more reliable, as long-lasting trends tend to be conserved in such potentially diagenetically-altered situations. The absence of correlation between the $\delta^{13}C_{carb}$ and $\delta^{13}C_{org}$ curves do not support this idea. The only common features between the two curves is an increase of 2 permil in $\delta^{13}C_{carb}$ and 0.7 permil in $\delta^{13}C_{org}$ at around beds 24 to 26 at BBR, i.e. above the T3 turnover and the FAD of *H. austriaca*. This could also be due to diagenetic influence, but this could also represent a more global signal, albeit apparently later than at PM. It is also important to note that the sampling frequency for $\delta^{13}C_{carb}$ at BBR is significantly higher than that of $\delta^{13}C_{org}$ at BBR, and either proxy at PM. Hence, the isotope signal in the PM section could perhaps have missed some features seen in the BBR section.

Concerning other sections: Unpublished data (of Richoz) from the Kaavalani and Bolücektasi Tepe sections from Turkey (see Gallet et al., 1992; 2002 for section details) do show a small but consistent increase of 0.4 permil in $\delta^{13}C_{carb}$ just below the FO of *H. austriaca*, at the top of equivalent magnetozone PM4r (Figs. 9,13). Korte et al. (2005) also present an increase in $\delta^{13}C_{carb}$ for the Silicka Brezova section of 0.6 permil, which should be around the FO of *H. austriaca* at the base of equivalent magnetozone PM5n. It is possible the chemostratigraphy and bio-magnetostratigraphy may be displaced with respect to each other at Silicka Brezova. Gawlick and Böhm (2000) also show a 0.5 permil increase in $\delta^{13}C_{carb}$ around the CNB in Austria, but it is not well stratigraphically constrained and corresponds exactly to a lithologic change.

Hence, at the upperpart of this 'potentially correlative increase' the $\delta^{13}C_{carb}$ values are ca. -0.5 in BBR, 2.6 in PM, 3.5 in Bolücektasi Tepe, 3.8 in Kaavalani; and around 3.7 permil in Silcka Brezeva (Korte et al., 2005). The amplitude of change in $\delta^{13}C_{carb}$ is around 0.4 in Turkey, 0.7 at PM and 0.7 in $\delta^{13}C_{org}$ in BBR; but around 2 permil in $\delta^{13}C_{carb}$ in BBR. At BBR the far larger amplitude rise in $\delta^{13}C_{carb}$ indicates either the presence of diagenesis, or modification of a global signal by local effects. In terms of timing, it seems this 'potentially correlative increase' appears around the FAD of *Me. parvus* at PM (at the top of magnetozone PM4n); below the FO of *H. austriaca* at the top of equivalent magnetozone PM4r in Turkey, and above the FO of *H. austriaca* at BBR and Silicka Brezeva (here base of equivalent of PM5n). However, all sections with a clear positive trend are in the Western Tethys Ocean. The existence of a truly global, stratigraphically useful $\delta^{13}C_{carb}$ signal at the CNB would need a clearer signal to be gathered from sections in other oceans. Indeed, it has been demonstrated for other time intervals that $\delta^{13}C$ signals for the Tethys Ocean commonly do not reflect those seen in the Panthalassa Ocean.

Hence, the $\delta^{13}C$ signal around the boundary interval varies greatly between sections, with some showing a positive excursion, others a negative shift, and others no signal at all. The $\delta^{13}C$ increase observed in some sections is apparently positioned at different stratigraphic levels between localities

and is also of a generally small amplitude, the size of which is typical of diagenetic or lithologic influence on the signal and within the range typical of regional primary influence. Rigo et al. (2012b) showed that PM is situated in an upwelling zone. Variations in upwelling strength in modern oceans can produce the same kind of amplitude in $\delta^{13}C$ we see here. So perhaps we have a global trend toward more positive values, but it is rather weak and influenced by local factors, and with different timing in its onset.

4.3.2. The oxygen and strontium isotopes:

Here the signal of oxygen isotopes analysed from conodont material seems to be resistant to diagenesis at both BBR and PM. As stated in Rigo et al. (2012b) the signal at PM is probably not global but represents the presence of an upwelling zone. The short-term increase in temperature at the boundary at BBR (Sun et al., 2020) has not been reproduced elsewhere, so far, and could also represent a regional event rather than a global one.

The decrease in temperature observed in the early Norian can be recognized at BBR (Sun et al., 2020), and seems to occur globally (except at PM). Its onset is rather close to the FO of *H. austriaca*; however, its position is not enough well defined at the moment to be a useful stratigraphic marker.

As Onoue et al. (2016) suggested the Sr isotope ratios in BBR are significantly higher than the expected seawater ratios due to thermal alteration. The data from PM probably have oceanic values. Whatever primary GSSP datum is chosen, either section shows a decreasing trend across the boundary (Onoue et al., 2018).

In summary, except perhaps a transient temperature increase (if it could be found outside BBR), there is little evidence for any major synchronous chemostratigraphic event at the CNB that could be recognized across all sections. The $\delta^{13}C$ signal at the CNB is highly variable across localities. A positive shift in $\delta^{13}C$ is observed in several sections and may reflect a global change, but even when present is typically so small that it could be explained as the result of weak diagenesis, or lithological change. In a broader view, either of the proposed datum are in a trend of decreasing Sr isotopes and around the onset of an increase in oxygen isotopes. Ultimately, chemostratigraphy does not appear to provide much solid help with correlation and deciding which GSSP datum is most suitable.

(Richoz, Golding, Lei et al.)

4.4. Is the stratigraphic record at Black Bear Ridge incomplete?

Using the same meter scale for both PM and BBR shows the approximate 2.4 to 1 expansion in the accumulation rate at PM compared to BBR (Fig. 16) (this is 5.3 to 1 over the range of *Me. parvus*; Table 3). The easiest way to compare the accumulation rate of two sections recording the same bioevents, is by using graphic correlation (Fig. 17). Flat levels in the line of correlation (LOC) imply a missing interval (referred to as a terrace), here marked as possible terraces TA and TB in Fig. 17. Above and below these terraces are two groups of events whose position in the same trend suggests these events are coeval or nearly coeval in both sections:

- The lower coeval group includes turnovers T1 and T2, LO of *Anatropites*, FO of *Me. communisti*, and FO of *Me. parvus* alfa. The FO of *M. dylani* is out of trend, indicating that this event is diachronous in the two sections.
- The upper coeval group includes LO of *Me. parvus* alfa, LO of *H. radiata*, LO of *H. austriaca* and possibly the LO of *Me. communisti*. The LO of this latter species is recorded for sure in level FNP138.1 at PM, but a single specimen of *Me.* cf. *communisti* has been found in level NA43 (Mazza et al., 2018, tab.1).

Terraces TA and TB can be detected in narrow intervals between the 1st and the 2nd coeval trends (Fig. 17). Terrace TA is located between turnover T2, the FO of *Me. parvus* beta and the FO of *H. austriaca*. Terrace TB is identified by turnover T3, the LAD of *M. parvus* alfa and the LAD of *H. radiata*. Terraces TA and TB suggest possible condensation at BBR, in beds 18 and 21. Considering that the setting of BBR is in the deepest portion of the Williston Basin, and that the transgression in the surrounding areas took place around the CNB interval (e.g., Zonneveld et al., 2010; Fig. 18), these terraces could be interpreted as non-depositional surfaces.

The position of the two non-depositional surfaces appears to be confirmed by the extraordinarily accurate numerical analysis of the conodont faunas provided by Orchard (2014, fig. 6). Figure 19 shows that the two non-depositional surfaces are in the two narrow intervals with the highest concentration of conodont last occurrences.

(Balini)

4.4.1 Is there sedimentological evidence of hiatus?

The inference of hiatus (hence possible erosion) at BBR using graphic correlation techniques (Fig. 17), is at odds with the sedimentology and palaeoenvironmental setting. The BBR section has been studied intensely, and no evidence of erosion or scour or contour currents or other current events in the boundary interval have been found. This is also the case for many metres above and below. This succession was deposited in a quiescent offshore depositional setting. Also, the boundary interval occurs within the Pardonet Formation, some 17 m above its contact with the underlying Ludington Formation (Fig. 18). Sedimentation rates were quite low through the CNB interval (i.e. demonstrated in Fig. 16), and, as a result, conodont collections are well-preserved, abundant and diverse.

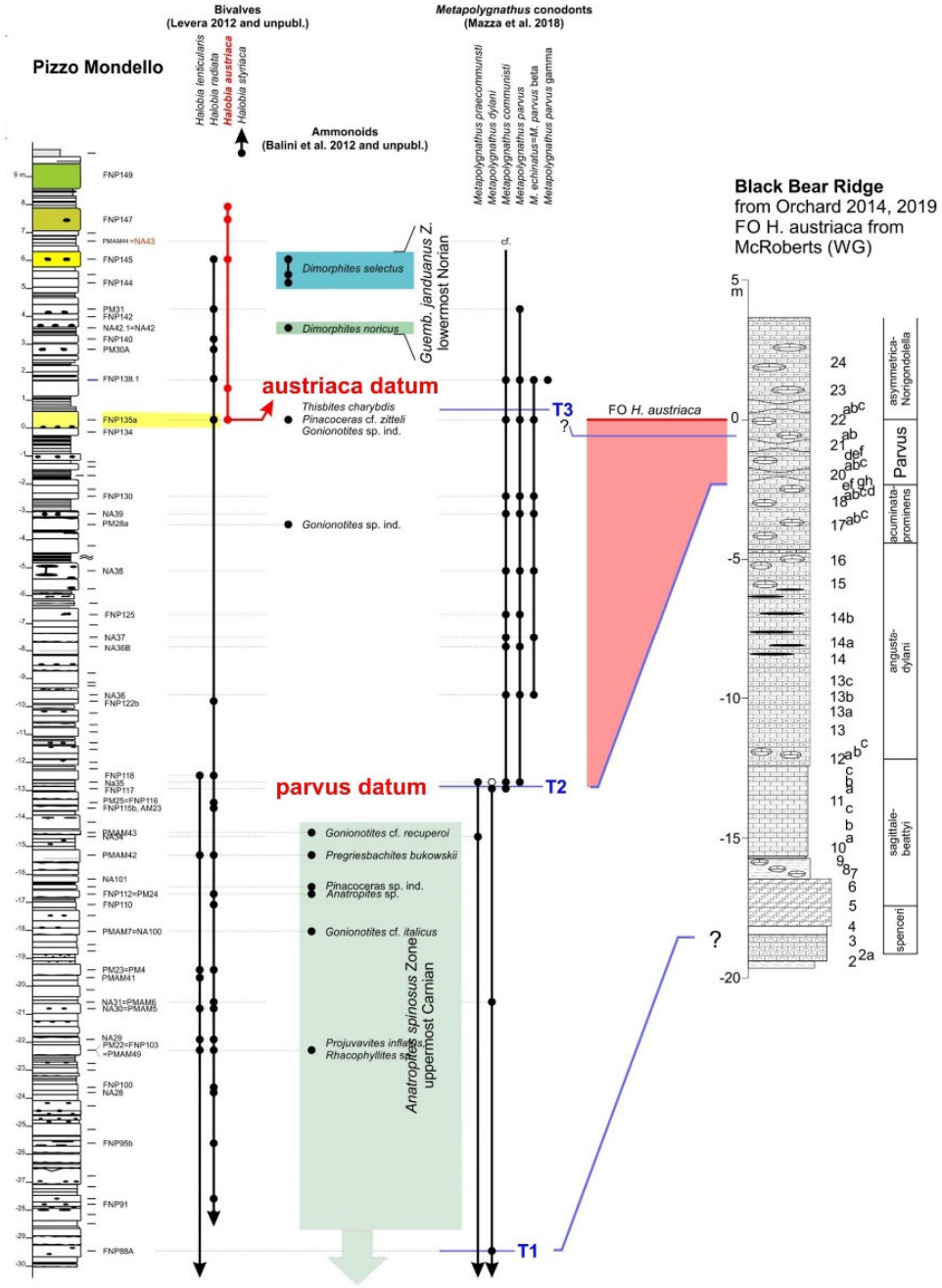

Figure 16. Tentative correlation of Pizzo Mondello and Black Bear Ridge sections, using the same meter scale for both logs. BBR log is from Orchard (2014), zonation and tentative position of conodont turnover events T1, T2 and T3 are from Orchard (2019). (Balini)

The Baldonnel Formation occurs primarily in the eastern part of the outcrop belt of the W. Canada Sedimentary Basin and does represent shallower water deposition (a shallow mixed siliciclastic-carbonate ramp succession). This formation is not present at BBR, but occurs on Williston Lake at the Pardonet Hill East, Brown Hill, McLay Spur, East Carbon Creek and West Schooler Creek sites, which are very different from each other. The Pardonet Hill East section occurs a few Km's from BBR, and the sections are rather different (Fig. 18) since they occur on different thrust sheets and were moved closer together during post-Triassic tectonism. Everywhere the Pardonet Formation represents distal offshore, deep-water deposition (even in eastern, more proximal settings). Also, the palaeogeography indicates that during the time of the CNB interval the location of the Black Bear Ridge section was ca.

150 to 200 km offshore from the nearest shoreline. Therefore, the likelihood of a sedimentation hiatus in the section is very low.

(Zonneveld)

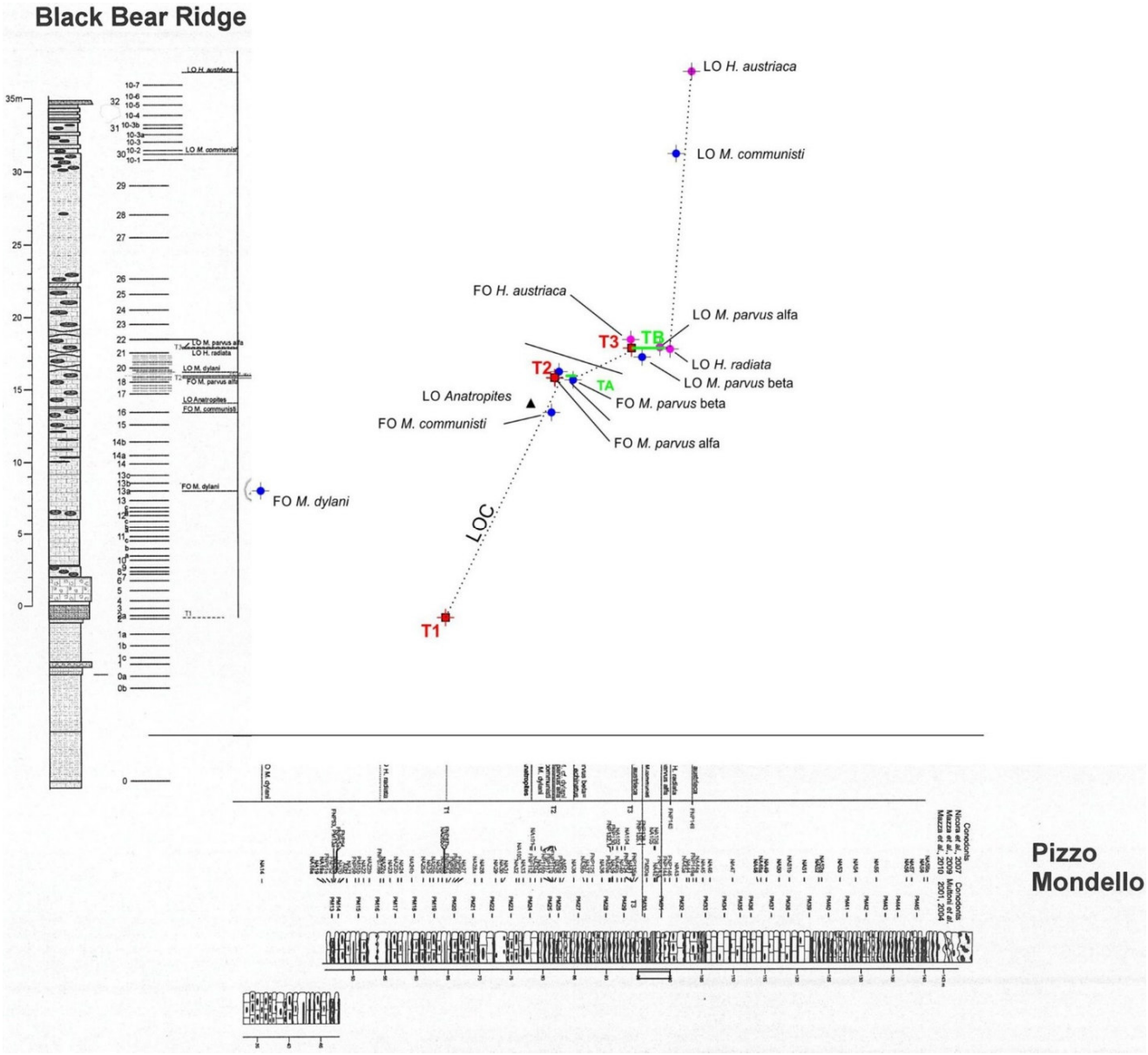

Fig. 17. Graphic correlation of first and last occurrence (FO and LO) events between BBR and PM. LOC=line of correlation (Balini).

4.4.2 The veracity of the conodont datums used in the graphic correlation

There is no doubt that the three turnover events (T1, T2, T) are recognized at both BBR and PM (Figs. 8,12, 16), but the basis for the exact positioning of the turnover T1 and T3 differs in the two sections, probably leading to some 'apparent diachroneity' in their exact placement. The turnover events T1, T2, and T3 were originally based on the PM conodont succession, and the FO and LO of the cohort of conodonts.

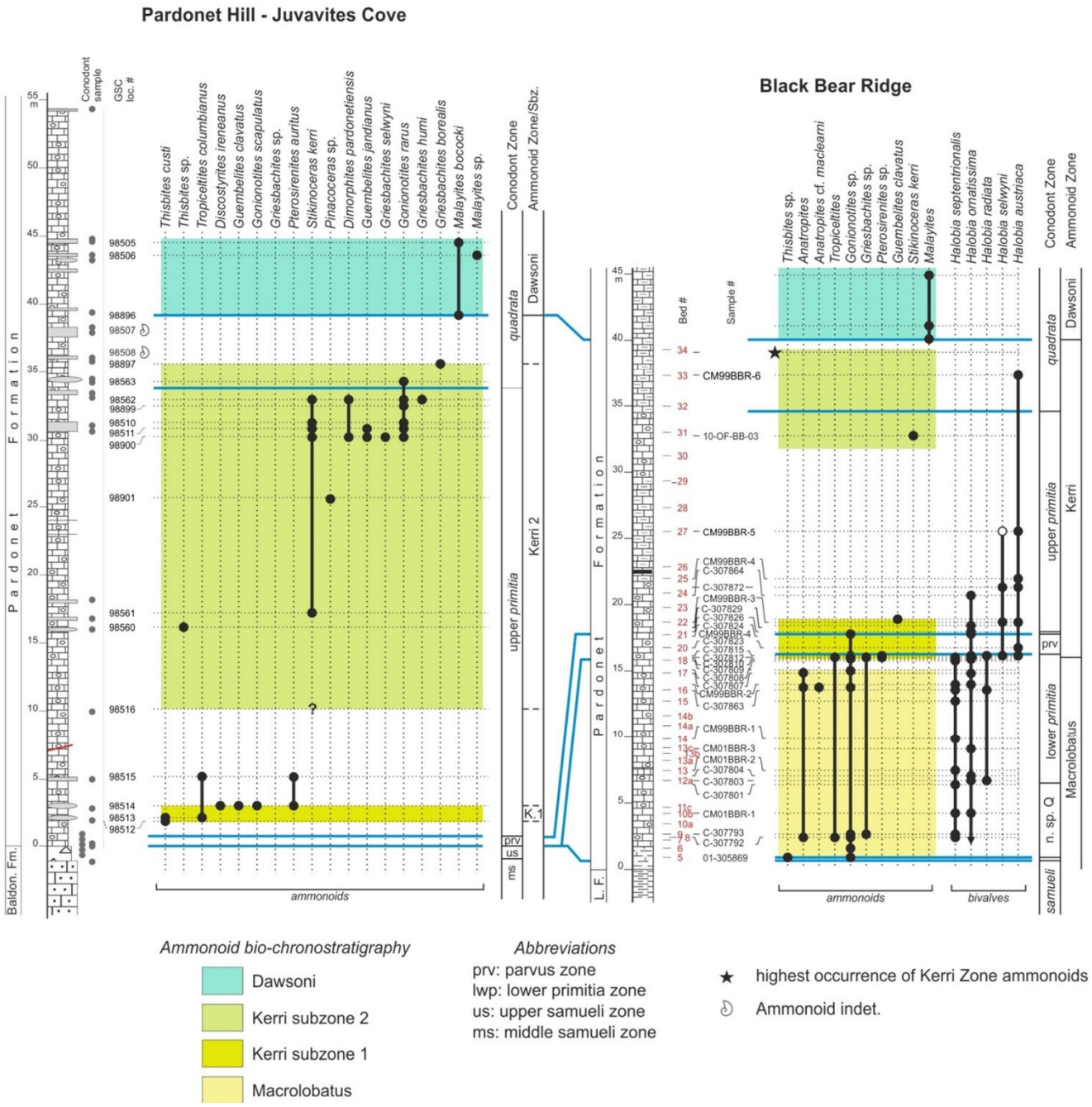

Fig. 18. Correlation of the Juvavites Cove (Pardonet Hill East) and Black Bear Ridge sections (from Balini et al. 2015, fig. 13). The Parvus Zone is documented at the very base of Pardonet Formation, thus documenting that the transgression of the Pardonet Formation on the Baldonnel Formation (at Pardonet Hill) took place at the beginning of the Kerri zone, and slightly later in the formation at BBR. L.F= Luddington Fm. In this figure the lower boundary of the Kerri subzone-1 is placed at the FO of *Pterosirenites*, although the chronostratigraphic significance of this event is not calibrated (Balini et al. 2012). The distribution of *Halobia* in this figure is also not that recently suggested by McRoberts (in press)- see Fig. 12.

The T1 event at PM was based on the replacement of *Carnepigondolella* by '*Epigondolella*', which is manifest as the *'C'. orchardi – 'E'. vialovi* zonal boundary at PM (Mazza et al., 2010). Orchard (2014) noted a significant turnover at the top of the *samueli* Zone at BBR (the 'BBR event datum'), where *Carnepigondolella* is replaced by *Primatella*. Consideration of the taxonomy of the '*Epigondolella*' species at PM led Orchard (2019, fig. 3) to revise the correlation of the BBR event datum to a position

within the *vialovi* Zone. Hence, the precise placement of the BBR datum at PM is unclear (for details, see Orchard, 2019, p. 53), so any correlation at this turnover may be diachronous.

The T2 event at PM was originally placed at the level at which *Metapolygnathus* became dominant over '*Epigondolella*' (Mazza et al., 2010), which was placed within the *communisti* Zone at PM. New definitions (Mazza et al., 2018) reduced the latter zone to a single bed and placed turnover T2 at the FO of *Me. parvus*. Hence, in agreement, the revised T2 now correlates with the base of the *parvus* Subzone at BBR, so chronostratigraphic correlation at this level may be near-synchronous.

The T3 event at PM was originally identified by *Metapolygnathus* largely disappearing and being replaced with advanced '*Epigondolella'* (probably *Primatella*) plus *Norigondolella.* These characteristics also identify the base of the *P. asymmetrica-Norigondolella* Subzone of Orchard (2014) at BBR. However, the re-definition of T3 as the base of the *Carnepigondolella*? *gulloae* Zone of Rigo et al. (2018) confuses the picture because this position is lower than the top of the *parvus* Zone at PM and therefore not directly correlated with BBR, because the species *gulloae* has been interpreted to lie within a spectrum of *Primatella* species (Orchard, 2019, p. 61), so correlation using this turnover may be diachronous.

Other taxa used in Fig. 17: *Metapolygnathus communisti* is rare at BBR, where Orchard (2014, fig. 46) differentiated five uncommon but different morphotypes that occurred in isolated beds through much of the Upper Carnian section. They were grouped as *Me.* ex gr. *communisti* and characterized by an anteriorly shifted pit and either a lack of, or poorly developed, anterior nodes, as per the definition of Mazza et al. (2012a). Later, Mazza et al. (2018) assigned most of the morphotypes to an extraordinarily broad species *M. praecommunisti*, but Orchard believes older representatives of *Me.* ex gr. *communisti* gave rise to *Me. dylani*, whereas a parallel development saw *Quadralella praecommunisti* developed from *Q. noah* and similar forms (Orchard, 2014, figs. 8, 13). Hence, the occurrence (and FO, LO) of *Me. communisti* sensu stricto at BBR is poorly constrained, so correlation at this level is almost certainty diachronous.

***Metapolygnathus dylani*.** Representatives, including the types of this species from BBR, are mostly inornate like those of its forbearer, *Me.* ex gr. *communisti*, whereas many of those illustrated from PM have nodes (Mazza et al., 2018). Interpreted in this broad way, this species may have a different range in the two sections (See Orchard 2019, p. 60, for details), readily accounting for its apparent diachroneity in the graphic correlation (Fig. 17).

***Metapolygnathus parvus*, morphotypes.** Both Orchard (2014) and Mazza et al. (2018) recognized three morphotypes of this species, but two of the three do not correspond (Orchard 2019, p. 55). The elongate beta morphotype, which lacks strong nodes or denticles, was erroneously called *Me. echinatus* by Orchard (2007), a determination that was followed by Mazza et al. (2012b, 2018) who included in the morphotype additional elements with a distinctive pair of anterior nodes or denticles. These latter elements were assigned to *Pa. destinae* by Orchard (2014), so the occurrence of *Me. parvus* beta morphotype at PM is unverified. Similarly, the gamma morphotype of *Me. parvus* described by Orchard (2014) has a much longer posterior process than that illustrated by Mazza et al. (2018) and is not clearly the same taxon. The subrectangular-oval alpha morphotype, close to the holotype of the species, is the more stable concept and occurs in both sections, hence the proposal in Section 2 as the potential CNB datum.

Hence, any graphic correlation (i.e., Fig. 17) needs to consider the probable diachroneity and uncertainty of some of these taxa 'datums'. A more realistic and holistic approach would place three best-fit straight lines to the data in Fig. 17, in so doing remove the very small terraces TA and TB from the likely line of correlation. Although sharing many taxa with BBR, the conodont-based correlation with Pizzo Mondello both within and above the *parvus* interval are rather more problematic (Orchard, 2019).

The entire Pardonet Formation at BBR is relatively condensed, but the completeness of the fossil succession is globally unrivalled. The cm scale sampling of the boundary beds at BBR has enabled the development of a refined temporal framework supported by detailed conodont morphogenesis (Orchard, 2014). The inference of hiatus at BBR from the graphic correlation shown in Fig. 17 therefore seems unfounded.

The number of conodont LAD and FAD in Fig. 19 reflect the relative 'taxonomic splitting', something that is concealed in the taxonomic 'lumping' at PM. The turnovers may not be very different if the taxonomies were fully aligned in both sections? An alternate explanation for the faunal turnovers (based on oxygen isotopes from BBR conodont elements), is a marked increase in temperature in the lower part of the *parvus* Subzone, and a return to 'normal' temperatures in the *asymmetrica-Norigondolella* Subzone (Sun et al., 2020). i.e., a climatic control of the turnovers rather than any hiatus.

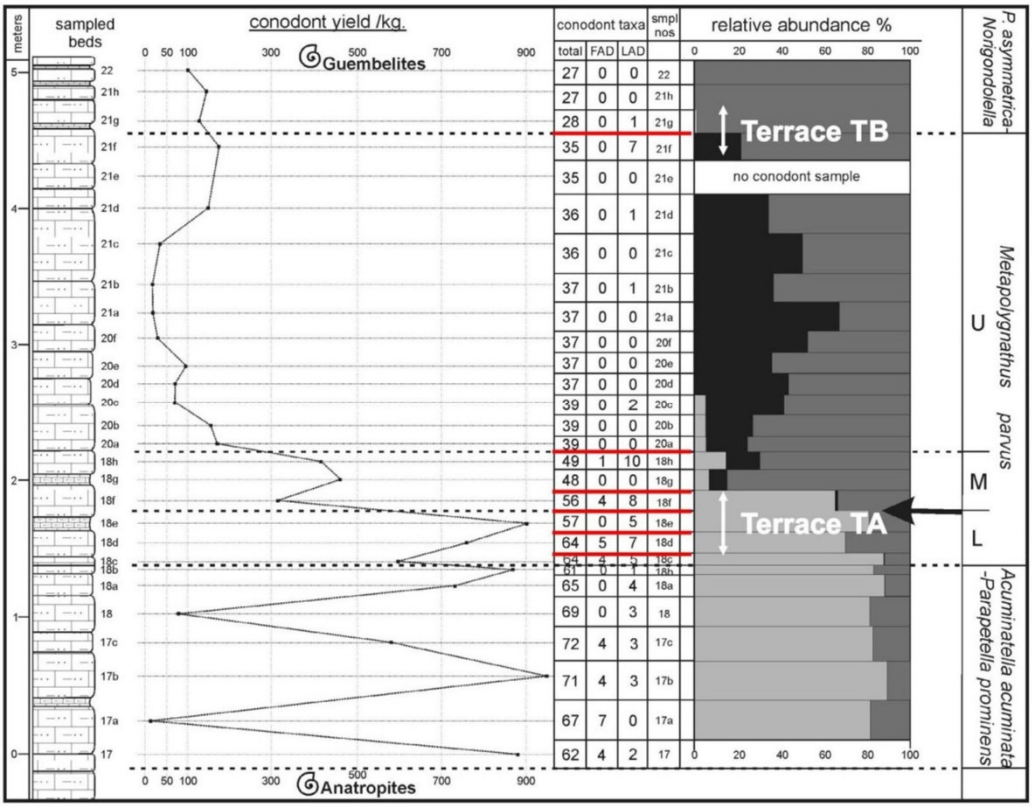

Fig. 19. Conodont faunas at BBR (from Orchard, 2014; fig. 6). The position of the inferred terraces TA and TB coincides with two intervals with highest number of LADs. In red, the bed surfaces with number of LADs greater than 4.

(Orchard)

4.5. Using the *H. austriaca* datum promotes biochronological stability

In North America, the 'standard' ammonoid chronology around the CNB are the zones of the 'latest Carnian' *Klamathites macrolobatus* and 'earliest Norian' *Stikinoceras kerri* (Tozer, 1994). From

studies dating back 50 years the Kerri Zone is consistently characterized by species of *Primatella* and *Norigondolella* conodonts. It has been shown that the Macrolobatus Zone is more diverse and includes several evolving conodont lineages divided into subzones at BBR (e.g., Fig. 14), with the youngest being the *parvus* Subzone and its Lower, Middle and Upper sub-divisions (Orchard, 2014).

At BBR, ca. 5 m of Pardonet Formation strata separates Macrolobatus and Kerri Zone ammonoid indicators (Fig. 18), which includes all of the *parvus* Subzone. Therefore, the ammonoid zonal position of the *parvus* Subzone at BBR is unfixed (using the FO of *Pterosirenites* for the base of the Kerri Zone as in Fig. 18 is highly speculative). However, from elsewhere in British Columbia, *parvus* Subzone conodonts are only known in association with Macrolobatus Zone ammonoids, which suggests the FAD of *Metapolygnathus parvus* lies within the Macrolobatus Zone (i.e., not as in Fig. 18). Therefore, if using the FAD of *Me. parvus* for the base of the Norian, part of this traditionally Carnian age ammonoid zone would be earliest Norian.

All strata overlying the *parvus* Subzone in North America contain the conodont associates *Primatella* and *Norigondolella*, which widely occur in the Kerri Zone. At BBR, the top of the *parvus* Subzone/ base of the succeeding *asymmetrica- Norigondolella* Subzone, the FO of the Kerri Zone ammonoid *Guembelites*, and the FO of *Halobia austriaca* (revised by McRoberts, in press) are all within about half a metre (Fig. 12). This revision of the halobiids brings into close alignment traditional Norian indicators and provides several proxies for a CNB that could be defined at around this level. Unfortunately, because only conodont last occurrences are known, no index conodont FAD can be proposed.

In summary, the *H. austriaca* datum for the base Norian definition, better preserves the N. American biochronostratigraphic tradition. This level would also consolidate the expected Carnian range of several conodont genera, with this boundary post-dating or very near their final demise. Also, at BBR this level broadly corresponds to a cooling event after marine temperature fluctuations in the *parvus* Subzone (Sun et al., 2020). It is also towards the end of an excursion interval in the carbonate $\delta^{13}C$ record that suggests ecosystem instability around the *parvus* Subzone (Lei et al., 2021). The succession at BBR also enables conodont-based correlation of the CNB with NE Asian Boreal regions where *Norigondolella navicula* occurs alone in the lower Norian of northern Siberia (Konstantinov et al., 2003). Similar sirenitid ammonoids present in the BBR section but unknown in Tethys provide further correlation potential (Section 4.2). Therefore, BBR provides an essential link between Boreal and Tethyan faunas (Konstantinov & Klets, 2009, Section 4.2).

(Orchard)

5. THE OUTCOME OF FORMAL VOTING WITHIN THE WORKING GROUP.

The Norian boundary working group was asked to rank the four options (as below, Table 3) for the boundary position. This unusual ICS voting procedure (due to the four options available) was cleared by the ICS executive.

Option A: The first occurrence of *Metapolygnathus parvus* at Pizzo Mondello
Option B: The first occurrence of *Halobia austriaca* at Black Bear Ridge
Option C: The first occurrence of *Halobia austriaca* at Pizzo Mondello
Option D: The first occurrence of *Metapolygnathus parvus* at Black Bear Ridge

By the deadline of midnight (GMT) on 6th May 2021, 24 of the 25 members of the CNB working group had voted (96% of members). The rankings were converted to scores by assigning rankings of 1 to 4

with the scores of 4 to 1, respectively (i.e. rank 1=score of 4; rank 4= score of 1, etc.). The cumulative scores for the four options were:

Option A	58
Option B	57
Option C	68
Option D	51

This made Option A and C move to the second round of voting. Although it made no difference for the outcome of this vote, if the scores of only ranks 1 and 2 are counted (i.e. first and second choices), the following scores would be obtained for the options, A=46, B=42, C=53, D=24, which also indicates the same preference for Options A and C.

Following the first round of voting, one of the two options listed below were voted-on for the base-Norian GSSP position. Therefore, Options A and C (as below, Table 3) formed the second round of voting, and the results of this second ballot are indicated below. By the voting deadline of midnight (GMT) on 26th July 2021, 20 of the 25 members of the CNB working group had voted (80% of members). The ballot results were:

Option A	8 ballots cast (40% of those who voted)
Option C	12 ballots cast (60% of those who voted)

Those voting for Option A were, Bachmann, Benton, Nicora, Onoue, Rigo, Tekin, Zhang and Zonneveld, and those voting for Option-C were: Balini, Carter, Golding, Hounslow, Konstantinov, Krystyn, Lucas, McRoberts, Muttoni, Orchard, Richoz, Sun.

Both the number of ballots cast and majority of votes (both set at 60% by ICS voting rules), makes Option C the choice selected by the working group to define the base of the Norian. That is the first occurrence of *Halobia austriaca* in the Pizzo Mondello section is the suggested GSSP 'golden spike' for the Norian (Table 3).

CONCLUSIONS

The first occurrence of *Halobia austriaca* at Pizzo Mondello has been chosen by the Carnian-Norian boundary working group as the primary datum for the base of the Norian. This will be put forward to the STS as the formal proposal for the base Norian GSSP. This level corresponds to the base of bed FNP135A at Pizzo Modello. The placement at this level in many ways embodies the historical precedence of the ammonoid zonations widely used in the Late Triassic, since this level, whilst not exactly equivalent, is close to the base of the traditional Norian in North America, Europe and probably in the Boreal realm in NE Asia. Closely associated potential secondary markers for the boundary in the section include: 1) the lower part of magnetozone PM5n, allowing correlation into terrestrial systems and those not bearing suitable fossils; and 2) the major turnover of conodonts (event T3) near the top of the Parvus Zone.

REFERENCES

Balini, M., Bertinelli, A., Di Stefano, P., Dumitrica, P., Furin, S., Gullo, M., Guaiumi, C., Hungerbuehler, A., Levera, M., Mazza, M., McRoberts, C.A., Muttoni, G., Nicora, A., Preto, N. & Rigo, M. 2008, Integrated stratigraphy of the Norian GSSP candidate Pizzo Mondello section (Sicani Mountains, Sicily): Berichte der Geologischen Bundesanstalt, 76: 23-25.

Balini, M., Bertinelli A., Di Stefano P., Guaiumi C., Levera M., Mazza M., Muttoni G., Nicora A., Preto N. & Rigo M. 2010. The Late Carnian-Rhaetian succession at Pizzo Mondello (Sicani Mountains). Albertiana, 39: 36-58.

Balini, M., Krystyn L., Levera M. & Tripodo A. 2012. Late Carnian-early Norian ammonoids from the GSSP candidate section Pizzo Mondello (Sicani Mountains, Sicily). Rivista Italiana di Paleontologia e Stratigrafia, 118: 47-84.

Balini, M., Jenks J.F., Martin R., McRoberts C.A., Orchard M.J. & Silberling N.J. 2015. The Carnian/Norian boundary succession at Berlin-Ichthyosaur State Park (Upper Triassic, central Nevada, USA). Paläontologische Zeitschrift, 89: 399-433.

Bellanca, A., Di Stefano, P. & Neri, R. 1995. Sedimentology and isotope geochemistry of Carnian deep-water marl/limestone deposits from the Sicani Mountains, Sicily: Environmental implications and evidence for a planktonic source of lime mud. Palaeogeography, Palaeoclimatology, Palaeoecology, 114(1): 111-129.

Berg, H.C. & Cruz, E.L. 1982. Map and table describing fossil collections and related samples in the Ketchikan and Prince Rupert quadrangles, southeastern Alaska. US Geog Survey openfile report 82-1088, Ancorage, Alaska.

Blome, C.D. 1983. Upper Triassic Capnuchosphaeridae and Capnodocinae (Radiolaria) from east-central Oregon: Micropaleontology 2, 9: 11-49.

Blome, C.D. 1984. Upper Triassic Radiolaria and radiolarian zonation from western North America: Bulletins of American Paleontology, 85: 1-88.

Bucur, I.I. 2001. Upper Triassic deposits of the Vascau plateau. *In*, Bucur II, Filipescu S. & Sasaran E.(Eds). Algae and carbonate platforms in the western part of Romania. 4th Regional Meeting of IFAA, Cluj-Napoca, Romania, August 29-September 5, 2001. Field Trip Guidebook.

Buryi, G.I. 1996. Triassic conodonts from the cherts of Nadandaha Range, Northeast China. Acta Micropaleontologica Sinica, 13: 207-214.

Bychkov, Yu.M., Dagys, A.S., Efimova, A.F. & Polubotko, I.V. 1976. Atlas of Triassic Fauna and Flora of the Northeastern USSR, Moscow: Nedra [in Russian].

Campbell, H.J. 1994. The Triassic bivalves Daonella and Halobia in New Zealand, New Caledonia, and Svalbard (No. 66). Institute of Geological & Nuclear Sciences Ltd.

Carter, E.S. 1993. Biochronology and paleontology of uppermost Triassic (Rhaetian) radiolarians, Queen Charlotte Islands, British Columbia, Canada. Mémoires de Géologie (Lausanne), 11, 75pp.

Carter, E.S. & Orchard, M.J. 2000, Intercalibrated conodont-radiolarian biostratigraphy and potential datums for the Carnian-Norian boundary within the Upper Triassic Peril Formation, Queen Charlotte Islands, British Columbia. Geological Survey of Canada, Current Research 2000- A7, 11p.

Carter, E.S. & Orchard, M.J. 2011, Radiolarians and conodonts across the Carnian-Norian Boundary in Haida Gwaii, British Columbia: Canadian Paleontology Conference, Proceedings No. 9, Vancouver, BC, August 19-22, 2011, p. 15.

Carter, E. S. & Orchard, M. J. 2013. Intercalibration of conodont and radiolarian faunas from the Carnian-Norian boundary interval in Haida Gwaii, British Columbia, Canada. *In,* Tanner, L. H., Spielmann, J. A. & Lucas, S. G. (Eds.). The Triassic System: New Developments in Stratigraphy and Paleontology: Bulletin 61: 67-92, New Mexico Museum of Natural History and Science.

Carter, E.S., Orchard, M.J. & Tozer, E.T. 1989, Integrated ammonoid conodont- radiolarian biostratigraphy, Late Triassic Kunga Group, Queen Charlotte Islands, British Columbia: Geological Survey of Canada, Paper 89-1H, p. 23-30.

Charlton, T.R., Barber, A.J., McGowan, A.J., Nicoll, R.S., Roniewicz, E., Cook, S.E., Barkham, S.T. & Bird, P.R. 2009. The Triassic of Timor: Lithostratigraphy, chronostratigraphy and palaeogeography. Journal of Asian Earth Sciences, 36: 341-363.

Dagys, A.S., Arkhipov,Yu.V. & Bychkov,Yu.M. 1979. Stratigraphy of the Triassic System of the North-Eastern Asia, Moscow: Nauka [in Russian].

De Wever, P., Sanfilippo, A., Riedel, W.R. & Gruber, B. 1979. Triassic Radiolaria from Greece, Sicily and Turkey: Micropaleontology, 25: 193-209.

Del Piero, N., Rigaud, S., Takahashi, S., Poulton, S.W. & Martini, R. 2020. Unravelling the paleoecology of flat clams: new insights from an Upper Triassic halobiid bivalve. Global and Planetary Change, 190: 103195, doi.org/10.1016/j.gloplacha.2020.103195.

Fuller, L.R. 1986. General Geology of Triassic Rocks at Alaska Canyon in the Jackson Mountains, Humboldt County, Nevada (Msc dissertation, University of Nevada, Reno).

Gawlick, H.J. & Böhm, F. 2000. Sequence and isotope stratigraphy of Late Triassic distal periplatform limestones from the northern Calcareous Alps (Kälberstein Quarry, Berchtesgaden Hallstatt Zone). International Journal of Earth Sciences, 89: 108-129.

Gallet, Y., Besse, J., Krystyn, L., Marcoux, J. & Théveniaut, H. 1992. Magnetostratigraphy of the Late Triassic Bolücektas□Tepe section (southwestern Turkey): implications for changes in magnetic reversal frequency. Physics of the Earth and Planetary Interiors, 73: 85-108.

Gallet, Y., Besse, J., Krystyn, L., Marcoux, J., Guex, J. & Théveniaut, H. 2000. Magnetostratigraphy of the Kaavalani section (southwestern Turkey): Consequence for the origin of the Antalya Calcareous Nappes (Turkey) and for the Norian (Late Triassic) magnetic polarity timescale. Geophysical Research Letters: 27, 2033-2036.

Guaiumi, C. 2008. Sedimentology of Upper Triassic hemipelagic micrites (Lagonegro and Sicani basins). PhD Thesis, Padua Univ.

Hounslow, M.W. & Muttoni, G. 2010. The geomagnetic polarity timescale for the Triassic: linkage to stage boundary definitions. *In,* Lucas, S.G (ed). The Triassic timescale. Geological Society, London, Special Publications, 334: 61-102.

Hüsing, S.K., Deenen, M.H., Koopmans, J.G. & Krijgsman, W. 2011. Magnetostratigraphic dating of the proposed Rhaetian GSSP at Steinbergkogel (Upper Triassic, Austria): Implications for the Late Triassic time scale. Earth and Planetary Science Letters, 302: 203-216.

Jin, X., McRoberts, C.A, Shi, Z., Mietto, P., Rigo, M. Roghi, G., Manfrin, S., Franceschi, M. & Preto, N. 2019. The aftermath of the CPE and the Carnian–Norian transition in northwestern Sichuan Basin, South China Journal of the Geological Society, 176: 179–196

Katkov, S.M., Miller, E.L. & Toro, J. 2010. Structural assemblies and age of deformation in the western sector of the Anyui-Chukotka Fold System, Northeastern Asia. Geotectonics, 44: 424-442.

Kaufman, A.J. & Knoll, A.H. 1995. Neoproterozoic variations in the C-isotopic composition of seawater: stratigraphic and biogeochemical implications. Precambrian Research, 73: 27-49.

Kent, D. V., Olsen, P. E. & Muttoni, G. 2017. Astrochronostratigraphic polarity time scale (APTS) for the Late Triassic and Early Jurassic from continental sediments and correlation with standard marine stages. Earth-Science Reviews, 166: 153-180.

Khuc, V. & Huyen, D.T. 1998. Triassic correlation of the Southeast Asian mainland. Palaeogeography, Palaeoclimatology, Palaeoecology, 143: 285-291.

Khuc, V. 1991.Paleontological Atlas of Vietnam, vol. 3, Mollusca. 207 pp. Science and Technics Publishing.

Kiparisova, L.D. 1947. Atlas of the Index Forms of the Fossil Faunas of the USSR. Vol. 7: Triassic System, Moscow: Gosgeolizdat [in Russian].

Kolar-Jurkovsek T. 1982. Konodonti iz amfiklìnskìh skladov in baškega dolomita - Conodonts from Amphiclina beds and Baca dolomite. Geologija, 25: 167-188.

Komatsu, T., Shigeta, Y., Doan, H.D., Trinh, H.T., Nguyen, H.B., Nguyen, M.T., Kusuhashi, N., Tsuihiji, T., Maekawa, T., Legrand, J. & Manabe, M. 2017. Upper Triassic (Carnian) mollusks from the Suoi Bang Formation in Me area, Ninh Binh Province, northern Vietnam. Bulleton National Musuem Natural Science, Series. C, 43: 1–10.

Konstantinov, A. G. 2019. A New Ammonoid Zone of the Upper Carnian Substage in Northeastern Russia. Russian Journal of Pacific Geology, 13: 522–534.

Konstantinov, A. G. & Klets, E. S. 2009. Stage Boundaries of the Triassic in Northeast Asia. Stratigraphy and Geological Correlation, 17: 173-191.

Konstantinov, A. G. & Sobolev 2000a. Biostratigraphy of the Carnian and Lower Norian in Northeastern Russia. Paper 1. Description of Sections, and Stratigraphic Distribution of Cephalopods. Geology of the Pacific Ocean, 16: 1-30.

Konstantinov, A. G. & Sobolev 2000b. Biostratigraphic Scheme of the Carnian and Lower Norian in NE Russia. Paper 2. New Zonal Scales and Correlation. Geology of Pacific Ocean, 16: 643-666.

Konstantinov, A. G. Sobolev, E. S. & Klets, T. V. 2003. New Data on Fauna and Biostratigraphy of Norian Deposits in the Kotel'nyi Island (New Siberian Islands). Stratigraphy and Geological Correlation, 11: 231–243.

Korchinskaya, M.V. 1082. Explanatory Note to the Stratigraphic Scheme of Mesozoic (Triassic) of Svalbard, Leningrad: PGO 'Sevmorgeologiya' [in Russian].

Korte, C., Kozur, H.W. & Veizer, J. 2005. $\delta^{13}C$ and $\delta^{18}O$ values of Triassic brachiopods and carbonate rocks as proxies for coeval seawater and palaeotemperature. Palaeogeography, Palaeoclimatology, Palaeoecology, 226: 287-306.

Kristan-Tollmann, E., Barkham, S. & Gruber, B. 1987. Pötschenschichten, zlambachmergel (Hallstätter Obertrias) und liasfleckenmergel in zentraltimor, Nebst ihren faunenelementen. Mitteilungen der österreichischen geologischen Gesellschaft, 80: 229-285.

Krystyn, L. 1980. Stratigraphy of the Hallstatt region. Guidebook, Abstracts, Second European Conodont Symposium-ECOS II. Abhandlungen der Geologischen Bundesanstalt, 35: 69-98.

Krystyn, L. & Gallet, Y. 2002. Towards a Tethyan Carnian-Norian boundary GSSP. Albertiana, 27: 12-19.

Lamolda, M.A., Paul, C.R.C., Peryt, D. & Pons, J.M. 2014. The global boundary stratotype and section point (GSSP) for the base of the Santonian Stage,' Cantera de Margas', Olazagutia, northern Spain. Episodes, 37: 2-13.

Lei, J.Z.X., Husson, J.M., Golding, M.L., Orchard, M.J. & Zonneveld, J.-P. 2021. Stable carbon isotope record of carbonate across the Carnian–Norian boundary at the prospective GSSP section at Black Bear Ridge, British Columbia, Canada. Albertiana, 46: 1–10.

Levera, M. & McRoberts, C.A. 2008. Carnian/Norian halobiids from Pizzo Mondello succession (Sicani Mountains, Sicily). Berichte Geol. B.-A., 76 – Upper Triassic …Bad Goisern.

Levera, M. 2012. The halobiids from the Norian GSSP candidate section of Pizzo Mondello (Western Sicily, Italy): systematics and correlations. Rivista Italiana di Paleontologia e Stratigrafia, 118: 3-45.

Lin, L., Zhu, L., Pang, Y. & Sha, J. 2007. A new genus of Pergamidiidae (Bivalvia) from the Late Triassic of the Changtai-Gacun area, eastern Qinghai-Xizang Plateau, China. Journal of Asian Earth Sciences, 30: 108-112.

Lucas, S. G. 2010. The Triassic chronostratigraphic scale: history and status. *In*, Lucas, S.G (ed). The Triassic timescale. Geological Society, London, Special Publications, 334: 17-39.

MacKevett, E.M. 1971. Stratigraphy and General Geology of the McCarthy C-5 Quadrangle; Alaska. US. Geological Survey Bulletin 1323, US printing Office Washington.

Marshall, J.D. 1992. Climatic and oceanographic isotopic signals from the carbonate rock record and their preservation: Geological Magazine, 129: 143-160.

Mazza, M. & Krystyn L. 2015. The revised Upper Triassic conodont record of the Tethys: a new step towards a better definition of the conodont bioevents around the base of the Norian stage. Ber Inst Erdwiss K-F-Univ Graz, 21: 243

Mazza, M. & Martinez-Perez, C. 2015. Unravelling conodont (Conodonta) ontogenetic processes in the Late Triassic through growth series reconstructions and X-ray microtomography. Bollettino della Società Paleontologica Italiana, 54: 161-186.

Mazza, M. & Martínez-Pérez, C. 2016. Evolutionary convergence in conodonts revealed by Synchrotron-based Tomographic Microscopy. Palaeontologia Electronica 19.3.52A: 1–11 palaeo-electronica.org/content/2016/1710- conodont-x-ray-tomographies

Mazza, M., Furin, S., Spötl, C. & Rigo, M. 2010. Generic turnovers of Carnian/Norian conodonts: Climatic control or competition? Palaeogeography, Palaeoclimatology, Palaeoecology, 290: 120-137.

Mazza, M., Rigo, M. & Nicora, A. 2011. A new Metapolygnathus platform conodont species and its implications for Upper Carnian global correlations. Acta Palaeontologica Polonica, 56: 121-131.

Mazza, M., Rigo, M. & Gullo, M. 2012a. Taxonomy and biostratigraphic record of the Upper Triassic conodonts of the Pizzo Mondello section (western Sicily, Italy), GSSP candidate for the base of the Norian. Rivista Italiana di Paleontologia e Stratigrafia, 118: 85-130.

Mazza, M., Cau, A. & Rigo, M. 2012a. Application of numerical cladistic analyses to the Carnian–Norian conodonts: a new approach for phylogenetic interpretations. Journal of Systematic Palaeontology, 10: 401-422.

Mazza, M., Nicora, A. & Rigo, M. 2018. *Metapolygnathus parvus* Kozur, 1972 (Conodonta): a potential primary marker for the Norian GSSP (Upper Triassic). Bollettino della Società Paleontologica Italiana, 57: 81-101.

McRoberts, C.A. 1990. Systematic paleontology stratigraphic occurrence and paleoecology of halobiid bivalves from the Martin Bridge Formation (Upper Triassic) Wallowa Terrane Oregon. Graduate Student Theses, Dissertations & Professional Papers. 7438, Univ Montana. https://scholarworks.umt.edu/etd/7438.

McRoberts C.A. 2007. The halobid bivalve succession across a potential Carnian/Norian GSSP at Black Bear Ridge, Williston Lake, northeast British Columbia, Canada. Albertiana, 36: 142-145.

McRoberts, C. A. 2010. Biochronology of Triassic bivalves. In: Lucas, S.G (Ed.) The Triassic timescale. Geological Society, London, Special Publications, 334: 201–219.

McRoberts, C.A. 2011. Late Triassic Bivalvia (Chiefly Halobiidae and Monotidae) from the Pardonet Formation, Williston Lake Area, Northeastern British Columbia, Canada. Journal of Paleontology, 85: 613-664.

McRoberts, C.A. in press. *Halobia austriaca* in North America with a reappraisal of its distribution across the Carnian-Norian boundary interval at Black Bear Ridge (northeastern British Columbia, Canada). Albertiana.

McRoberts, C.A. & Krystyn, L. 2011. The FOD of *Halobia austriaca* at Black Bear Ridge (northeastern British Columbia) as the base-Norian GSSP. 21st Canadian Paleontology Conference, UBC, August 19–21, Proceedings 9: 38–9.

Meng, Q., Qu, H. & Hu, J. 2007. Triassic deep-marine sedimentation in the western Qinling and Songpan terrane. Science in China Series D: Earth Sciences, 50: 246-263.

Mietto, P., Jin, X., Manfrin, S., Lu, G., Shi, Z., Gianolla, P., Huang, X. & Preto, N. 2021. Onset of sedimentation near the Carnian/Norian boundary in the northwestern Sichuan Basin: New

evidence from ammonoid biostratigraphy and zircon UPb geochronology. Palaeogeography, Palaeoclimatology, Palaeoecology, 567: doi.org/10.1016/j.palaeo.2021.110246.

Mojsisovics, E. von. 1869. Über die Gliederung der oberen Triasbildungen der östlichen Alpen. Geologische Reichsanstalt. Jahrbuch, 24:91-150.

Mojsisovics, E. von. 1874. Über Die Triadischen Pelecypoden–Gattungen Daonella und Halobia. Abhandlungen der k. k. Geologischen Reichsanstalt, 7: 1–35

Montenat, C. 2009. The Mesozoic of Afghanistan. GeoArabia, 14: 147-210.

Muttoni G., Kent D.V., Di Stefano P., Gullo M., Nicora A., Tait J. & Lowrie W. 2001a. Magnetostratigraphy and biostratigraphy of the Carnian/Norian boundry interval from the Pizzo Mondello section (Sicani Mountains, Sicily). Palaeogeography, Palaeoclimatology, Palaeoecology, 166: 383-399.

Muttoni, G., Kent, D. V. & Orchard, M. J. 2001b. Paleomagnetic reconnaissance of early Mesozoic carbonates from Williston Lake, northeastern British Columbia, Canada: evidence for late Mesozoic remagnetization. Canadian Journal of Earth Sciences, 38:1157-1168.

Muttoni G., Kent D.V., Olsen P.E., Di Stefano P., Lowrie W., Bernasconi S.M. & Hernández F.M. 2004 Tethyan magnetostratigraphy from Pizzo Mondello (Sicily) and correlation to the Late Triassic Newark astrochronological polarity time scale. Geological Society America Bulletin, 116: 1043–1058.

Muttoni G., Mazza M., Mosher D., Katz M.E., Kent D.V. & Balini M. 2014. A Middle–Late Triassic (Ladinian–Rhaetian) carbon and oxygen isotope record from the Tethyan Ocean. Palaeogeography, Palaeoclimatology, Palaeoecology, 399: 246–259.

Nicora A., Balini M., Bellanca A., Bertinelli A., Bowring S.A., Di Stefano P., Dumitrica P., Guaiumi C., Gullo M., Hungerbuehler A., Levera M., Mazza M., McRoberts C.A., Muttoni G., Preto N. & Rigo M. 2007. The Carnian/Norian boundary interval at Pizzo Mondello (Sicani Mountains, Sicily) and its bearing for the definition of the GSSP of the Norian Stage. Albertiana, 36: 115-129.

Noyan O. & Kozur H. 2007. Revision of the late Carnian-early Norian conodonts from the Stefanion section (Argolis, Greece) and their paleobiogeographic implications. Neues Jahrbuch für Geologie und Paleontologie Abhandlungen, 245: 159-178.

Onoue, T., Zonneveld, J. P., Orchard, M. J., Yamashita, M., Yamashita, K., Sato, H. & Kusaka, S. 2016. Paleoenvironmental changes across the Carnian/Norian boundary in the Black Bear Ridge section, British Columbia, Canada. Palaeogeography, Palaeoclimatology, Palaeoecology, 441: 721-733.

Onoue, T., Yamashita, K., Fukuda, C., Soda, K., Tomimatsu, Y., Abate, B. & Rigo, M. 2018. Sr isotope variations in the Upper Triassic succession at Pizzo Mondello, Sicily: Constraints on the timing of the Cimmerian Orogeny. Palaeogeography, Palaeoclimatology, Palaeoecology, 499: 131-137.

Orchard, M.J. 2007. A proposed Carnian-Norian Boundary GSSP at Black Bear Ridge, northeast British Columbia, and a new conodont framework for the boundary interval. Albertiana, 36: 130-141.

Orchard, M.J. 2010. Triassic conodonts and their role in stage boundary definitions. *In* Lucas S.G. (ed.), The Triassic Timescale. Geological Society, Special Publication, 334: 139-161.

Orchard, M.J. 2013. Five new genera of conodonts from the Carnian-Norian boundary beds of Black Bear Ridge, northeast British Columbia, Canada. In: Tanner, L.H., Spielmann, J.A. and Lucas, S.G. (eds.), The Triassic system. New Mexico Museum of Natural History and Science Bulletin, 61, 445-457.

Orchard, M.J. 2014. Conodonts from the Carnian-Norian Boundary (Upper Triassic) of Black Bear Ridge, Northeastern British Columbia, Canada. New Mexico Museum of Natural History and Science Bullettin, 64, 139 pp.

Orchard, M.J. 2019. The Carnian-Norian boundary GSSP candidate at Black Bear Ridge, British Columbia, Canada: update, correlation, and conodont taxonomy. Albertiana, 45: 50-68.

Orchard, M.J., McRoberts, C.A., Tozer, E.T., Johns, M.J., Sandy, M.R. & Shaner, J.S. 2001. An intercalibrated biostratigraphy of the Upper Triassic of Black Bear Ridge, Williston Lake, northeast British Columbia. Natural Resources Canada, Geological Survey of Canada.

Orchard, M.J., Zonneveld, J.P., Johns, M.J., McRoberts, C.A., Sandy, M.R., Tozer, E.T. & Carrelli, G.G. 2001. Fossil succession and sequence stratigraphy of the Upper Triassic of Black Bear Ridge, Northeast British Columbia, a GSSP prospect for the Carnian–Norian boundary. Albertiana, 25: 10–22.

Paterson, N.W. & Mangerud, G. 2020. A revised palynozonation for the Middle–Upper Triassic (Anisian–Rhaetian) series of the Norwegian Arctic. Geological Magazine, 157: 1568-1592.

Polubotko, I.V. 2005. Halobiide based biozonation of the Upper Triassic in the Northeast Russia. In Mater. Vseross. nauchn. konf., posvyashch. pamyati akad. KV Simakova iv chest'ego 70-letiya 'Nauka Severo-Vostoka Rossii–nachalo veka' (Magadan, 26–28 april, 2005.), pp. 26-28.

Polubotko, I.V. 1986. Zonal complexes of Late Triassic halobiids in the northeastern USSR. In: Yanshin, A.L. (ed). Mesozoic Biostratigraphy of Siberia and the Far East. Transactions of the Institute of Geology and Geophysics, Novosibirsk, 648: 63-72 [in Russian].

Popescu, D.A. & Popescu, L.G. 2008. Microfacies of the Triassic limestones in the Izvorul Malului klippe (Rarău Syncline, Transylvanian Nappes, Eastern Carpathians, Romania). Georeview: Scientific Annals of Stefan cel Mare University of Suceava. Geography Series, 17: 113-131.

Preto, N., Agnini, C., Rigo, M., Sprovieri, M. & Westphal, H. 2013. The calcareous nannofossil Prinsiosphaera achieved rock-forming abundances in the latest Triassic of western Tethys: consequences for the δ 13 C of bulk carbonate. Rivista Italiana di Paleontologia e Stratigrafia, 118: 131-141.

Raine, J.I., Beu, A.G., Boyes, A.F., Campbell, H.J., Cooper, R.A., Crampton, J.S., Crundwell, M.P., Hollis, C.J. & Morgans, H.E.G. 2012. Revised calibration of the New Zealand geological timescale. NZGT2015/1. GNS Science report, 39: 1-53.

Riediger, C., Carrelli, G.G. & Zonneveld, J.P. 2004. Hydrocarbon source rock characterization and thermal maturity of the Upper Triassic Baldonnel and Pardonet formations, northeastern British Columbia, Canada. Bulletin of Canadian Petroleum Geology, 52: 277-301.

Rigo M., Preto N., Franceschi M. & Guaiumi C. 2012a. Stratigraphy of the Carnian-Norian Calcari con Selce Formation in the Lagonegro Basin, Southern Apennines. Rivista Italia Paleontologica Stratigraphy, 118: 143–154.

Rigo, M., Trotter, J.A., Preto, N. & Williams, I.S. 2012b. Oxygen isotopic evidence for Late Triassic monsoonal upwelling in the northwestern Tethys. Geology, 40: 515–518.

Rigo M., Mazza M., Karádi V. & Nicora A. 2018. New Upper Triassic conodont biozonation on of the Tethyan Realm. In: Tanner L.H. (ed.), The Late Triassic World: Earth in a Time of Transition, Topics in Geobiology 46: 189-235, Springer.

Seilacher, A. 1990. Aberrations in bivalve evolution related to photo-and chemosymbiosis. Historical Biology, 3: 289-311.

Sha, J. & Grant-Mackie, J.A. 1996. Late Permian to Miocene bivalve assemblages from Hohxil, Qinghai-Xizang Plateau, China. Journal of the Royal Society of New Zealand, 26: 429-455.

Shackleton, R.M., Ries, A.C., Bird, P.R., Filbrandt, J.B., Lee, C.W. & Cunningham, G.C. 1990. The Batain Melange of NE Oman. *In*, Robertson, A. H. F., Searle, M. P. & Raes, A. C. (eds), The Geology and Tectonics of the Oman Region. Geological Society Special Publication, 49: 673-696.

Silberling, N.J. 1963. Field guide to halobiid and monotid pelecypods of the Alaskan Triassic. US Geological Survey Open File Report, pp.1-9.

Smith, J.P. 1927. Upper Triassic marine invertebrate faunas of North America. US Geol. Survey, Professional paper 141. US Gov't. Printing Office.

Stanley, G.D., McRoberts, C.A. & Whalen, M.T. 2008. Stratigraphy of the Triassic Martin Bridge Formation, Wallowa terrane: stratigraphy and depositional setting. Geological Society of America Special Papers, 442: 227-250.

Sun, Y. D., Orchard, M. J., Kocsis, Á. T. & Joachimski, M. M. 2020. Carnian–Norian (Late Triassic) climate change: Evidence from conodont oxygen isotope thermometry with implications for reef development and Wrangellian tectonics. Earth and Planetary Science Letters, 534: doi.org/10.1016/j.epsl.2020.116082.

Tekin, U.K. & Yurtsever, T.S.,2003. Late Triassic (early to middle Norian) radiolarians from the Antalya nappes, Antalya, SW Turkey. Journal of Micropalaeontology, 22: 147-162.

Tozer, E.T. 1994. Canadian Triassic ammonoid faunas, Bulletin Geological Survey Canada, 467: 1–663.

Trotter J.A., Williams I.S., Nicora A., Mazza M. & Rigo M. 2015 Long-term cycles of Triassic climate change: a new $\delta^{18}O$ record from conodont apatite. Earth and Planetary Science Letters, 415: 165–174.

Truschelev, A.M. & Grinenko, V.S. 2016. Boreal Trias in the Yana and Indigirka rivers- new sheet Q-53 stratigraphy- Verkhoyansk. Bulletin of Goskomgeologii, 15: 33-75.

Tun Min, T. & Maung, M. 2019. Stratigraphy of Pane Chaung Group in Bhopi Vum Area, Tiddim Township, Chin State. The Third Myanmar National Conference on Earth Sciences (MNCES, 2019) November 7-8, Yadanabon University, Mandalay, Myanmar, pp. 186-194.

Visscher, H. & Krystyn, L. 1978. Aspects of Late Triassic palynology. 4. A palynological assemblage from ammonoid-controlled Late Karnian (Tuvalian) sediments of Sicily. Review of Palaeobotany and Palynology, 26: 93-112.

Vozin, V.F. & Tikhomirova,V.V. 1964. Field Atlas of Bivalves and Cephalopods from the Triassic Deposits of the Northeastern USSR, Moscow: Nauka [in Russian].

Wahyudiono, J., Susilo, A., Adlan, R., Salimudin, B., Gibran, A.K. & Wiratmoko, E.S. 2018. Integrated Field Mapping, Organic Chemistry and Subsurface Geological Interpretation of Kanikeh Formation as Potential Source Rock in Seram Island. Proceedings, Indonesian Petroleum Association, Forty-Second Annual Convention & Exhibition, May 2018, House, Hanoi.

Williford K.A., Orchard, M.J., Zonneveld, J.P. McRoberts, C.A. & Beatty, T.W. 2007. A record of stable organic carbon isotopes from the Carnian Norian boundary section at Black Bear Ridge, Williston Lake, British Columbia, Canada. Albertiana, 36: 146-148.

Yamashita D, Yasuda C, Ishibashi T., Martini R. & Onoue T. 2016. Stratigraphy and conodont and ammonoid ages of Upper Triassic Nakijin Formation in Hedomisaki area, Okinawa-jima, Japan. Journal Geological Society Japan, 122: 477–493.

Zonneveld, J. P., Beatty, T. W., Williford, K. H., Orchard, M. J. & McRoberts, C. A. 2010. Stratigraphy and sedimentology of the lower Black Bear Ridge section, British Columbia: candidate for the base-Norian GSSP. Stratigraphy, 7: 61-82.